

# Two modes of inhibitory neuronal shutdown distinctly amplify seizures in humans

## AUTHORS

Omar J. Ahmed<sup>1,2,3,4,5,14,15,#</sup>, Tibin T. John<sup>1,2,15</sup>, Shyam K. Sudhakar<sup>1</sup>, Ellen K.W. Brennan<sup>1,2</sup>, Alcides Lorenzo Gonzalez<sup>1,2</sup>, Jason S. Naftulin<sup>8</sup>, Emad Eskandar<sup>9</sup>, Joseph R. Madsen<sup>10</sup>, G. Rees Cosgrove<sup>11</sup>, Andrew S. Blum<sup>12</sup>, N. Stevenson Potter<sup>12</sup>, George A. Mashour<sup>6,7</sup>, Leigh R. Hochberg<sup>8,13</sup>, Sydney S. Cash<sup>8,14</sup>

## AFFILIATIONS

<sup>1</sup>Dept. of Psychology,

<sup>2</sup>Neuroscience Graduate Program,

<sup>3</sup>Michigan Center for Integrative Research in Critical Care,

<sup>4</sup>Kresge Hearing Research Institute,

<sup>5</sup>Dept. of Biomedical Engineering,

<sup>6</sup>Dept. of Anesthesiology,

<sup>7</sup>Dept. of Neurosurgery,

University of Michigan, Ann Arbor, MI 48109.

<sup>8</sup>Dept. of Neurology,

<sup>9</sup>Dept. of Neurosurgery,

Harvard Medical School and Massachusetts General Hospital, Boston, MA 02114

<sup>10</sup>Dept. of Neurosurgery,

Boston Children's Hospital, Boston, MA 02115

<sup>11</sup>Dept. of Neurosurgery,

Harvard Medical School and Brigham and Women's Hospital, Boston, MA 02115

<sup>12</sup>Dept. of Neurology,

Rhode Island Hospital, Providence, RI 02903

<sup>13</sup>School of Engineering, Brown University, Providence, RI 02912

<sup>14</sup>Co-senior authors

<sup>15</sup>Co-first authors

## #LEAD CONTACT & CORRESPONDING AUTHOR

Omar J. Ahmed

*Mail:* Department of Psychology, 530 Church St. University of Michigan, Ann Arbor, MI 48109

*Email:* ojahmed@umich.edu

**KEYWORDS:** inhibition, excitation, epilepsy, temporal lobe, mesial temporal sclerosis, neocortical dysplasia, neocortex, local field potential, human, depolarization block, spike and wave, secondary generalization, subthreshold dynamics

57 **ABSTRACT**

58 Inhibitory neurons are critical for normal brain function but dysregulated in disorders  
59 such as epilepsy. At least two theories exist for how inhibition may acutely decrease  
60 during a seizure: hyperpolarization of fast-spiking (FS) inhibitory neurons by other  
61 inhibitory neurons, or depolarization block (DB) of FS neurons resulting in an inability to  
62 fire action potentials. Firing rate alone is unable to disambiguate these alternatives.  
63 Here, we show that human FS neurons can stop firing due to both hyperpolarization and  
64 DB within the same seizure. However, only DB of FS cells is associated with dramatic  
65 increases in local seizure amplitude, unobstructed traveling waves, and transient  
66 increases in excitatory neuronal firing. This result is independent of seizure etiology or  
67 focus. Computational models of DB reproduce the *in vivo* human biophysics. These  
68 methods enable intracellular decoding using only extracellular recordings in humans  
69 and explain the otherwise ambiguous inhibitory neuronal control of human seizures.

70  
71

72

73

74

75

76

77

78

79

80

81

82

83

84

85

86

87

88 **INTRODUCTION**

89  
90 Epilepsy is a debilitating disease affecting some 50 million people worldwide<sup>1,2</sup>. Epileptic  
91 seizures are thought to result from an imbalance between excitatory and inhibitory  
92 neuronal activity<sup>3</sup>. However, electrographically similar seizures on the macroscopic  
93 scale can be driven by mechanistically distinct processes on the cellular and cell-type  
94 population scale<sup>4</sup>. Thus, the relative roles of local inhibitory and excitatory networks in  
95 driving seizure progression must be elucidated to guide the development of novel  
96 treatments for intractable epilepsies and our understanding of their associated seizures.  
97 Due to the tremendous technical challenges of recording from individual human neurons  
98 and the relative sparsity of inhibitory neurons, the activity of well isolated inhibitory  
99 interneurons during seizures is only rarely examined<sup>5,6</sup>.

100

101 There are several theories, based on slice and whole animal experiments, proposing  
102 both insufficient<sup>7–15</sup> and excessive<sup>16–20</sup> inhibition as possible facilitators of epileptic  
103 activity, with at least two hypotheses for how inhibition may acutely decrease during a  
104 seizure: (1) hyperpolarization of fast-spiking (FS) inhibitory neurons by other inhibitory  
105 neurons<sup>21–24</sup>, or (2) excessive depolarization of FS neurons that precludes subsequent  
106 action potentials due to blockade of voltage-dependent sodium channels<sup>12,14,25,56</sup>.  
107 Resolving these two theories necessitates whole cell recordings<sup>26</sup>, but it is practically  
108 impossible to record the intracellular membrane potential of neurons during human  
109 seizures *in vivo*. In this study, we address these challenges by combining (1) large-  
110 scale extracellular recordings of human neocortical inhibitory and excitatory neurons  
111 during focal seizures with secondary generalization and (2) a novel method of decoding

112 membrane potential trajectory from extracellular action potentials. We show the  
113 remarkable ability of active fast-spiking inhibitory neurons to block epileptic traveling  
114 waves in human neocortex, and reveal the dynamical control of human seizures by the  
115 subthreshold trajectory of inhibitory neurons.

116

117

118 **RESULTS**

119 Patients were implanted with intracranial grid electrodes as part of the clinical process  
120 of identifying the precise site of origin of their drug-resistant focal epilepsy (see  
121 Materials and Methods). A 4x4 mm NeuroPort microarray (Blackrock Microsystems)  
122 was also placed in a region of the neocortex that was expected to be in the resection  
123 site (Figure 1a; Extended Data Fig. 1a). Histology of the resected tissue confirmed that  
124 the electrodes consistently targeted layers 2/3 of the neocortex (Extended Data Fig. 1b).  
125 We used these arrays to simultaneously record the activity of dozens of individual  
126 neocortical neurons during both ictal and interictal activity. We then classified the  
127 neurons as either fast-spiking (FS) inhibitory interneurons or regular-spiking (RS)  
128 excitatory cells using well-established criteria<sup>27,28</sup>, including action potential shape  
129 (Extended Data Fig. 1c-f). FS cells correspond to the class of parvalbumin-expressing  
130 interneurons and represent the largest source of inhibition in the neocortex<sup>29</sup>. The  
131 resulting information thus allowed us to differentiate between putative inhibitory and  
132 excitatory unit activity patterns during seizure progression in humans.

133

134 A total of 37 FS cells and 539 RS cells were recorded across 4 patients with NeuroPort  
135 arrays implanted in the temporal neocortex (see Supplementary Methods for details  
136 about each patient). As secondarily generalized seizures first reached the arrays, both  
137 FS and RS cells increased their rate of action potentials (Figs. 1, 2, and Extended Data  
138 Figs. 2-4). This finding is consistent with what is known about the feedforward  
139 recruitment of both inhibition and excitation<sup>25,30</sup>. At the population level, the FS firing  
140 rate was significantly higher than RS cells (100,000 bootstrap iterations of label-shuffled

141 peak rate differences;  $p=0.036$ ). Within 40 seconds of seizure onset, the mean FS firing  
142 rate fell rapidly to 0-2 Hz at the same time as local field potential intensity increased  
143 dramatically to its highest levels (Figs. 1, 2, and Extended Data Figs. 2-4). Consistently,  
144 among the best isolated FS units during the seizure (isolation quality discussed in more  
145 detail below and see Methods), 10 out of 15 had at least one nearby RS cell that  
146 exhibited the peak of its overall activity several seconds after the dramatic fall in local  
147 FS activity and accompanying elevation in local field potential intensity (Figs. 1, 2, and  
148 Extended Data Figs. 2-4). Thus, at the population level, FS cells show a cessation of  
149 activity near the middle of secondarily generalized seizures accompanied by a dramatic  
150 increase in the amplitude of seizure activity. This FS cessation is followed by a transient  
151 increase in RS cell firing, presumably because these RS cells are now less inhibited  
152 due to the loss of FS firing. The RS population rate eventually also fell to an average of  
153 0-3 Hz but with a delay of several seconds following FS cells. At the population level,  
154 FS cells ( $N=37$ ) exhibited significantly earlier cessation times than RS cells ( $N=539$ )  
155 (Fig. 2g-j, FS cell average cessation occurred 4.6 seconds earlier than RS average  
156 cessation; 100,000 bootstrap iterations of label-shuffled time differences;  $p<0.0001$ ).

157  
158 We next compared activity patterns among individual FS cells. Many individual FS cells  
159 did not start firing until ~10 seconds into the seizure, often starting to fire robustly only  
160 after the RS rate had already increased (Figs. 1, 2, and Extended Data Figs. 2-4). As  
161 seen with the population means (Fig. 2g), each individual FS cell dramatically reduced  
162 its firing roughly half-way through the seizure (Figs. 1, 2, and Extended Data Figs. 2-4).  
163 However, even simultaneously recorded FS cells during a single seizure did not

164 necessarily cease firing at the same time, just as they did not start firing at the same  
165 time. Figure 1 shows the activity of two simultaneously recorded FS cells that were  
166 separated by a distance of 2.04 mm. FS Cell 1 (Fig. 1a) approached cessation ~35  
167 seconds into the seizure, and at ~35 seconds, the amplitude of the LFP next to FS Cell  
168 1 increased dramatically, as did the firing rate of nearby RS cells. FS Cell 2 (Fig. 1b)  
169 approached cessation ~24 seconds into the seizure, and the LFP amplitude next to FS  
170 Cell 2 also increased at ~24 seconds, along with the firing rate of nearby RS cells.  
171 Furthermore, when sorting all simultaneously recorded channels during a seizure by the  
172 timing of transition to the large amplitude spike-and-wave event phase, a raster plot of  
173 all spikes with units sorted in the same order produced a similar sequence of mid-  
174 seizure firing time cessations (Fig. 1c&d). Thus, FS cell cessation is correlated with a  
175 dramatic increase in the very local intensity of seizures.

176  
177 Given changing waveform shapes and noise characteristics during seizures<sup>31</sup>, an  
178 important methodological question arises of how separable clusters in waveform feature  
179 space are from each other and from noise to allow valid unit assignments during this  
180 period. To quantitatively assess this isolation quality of feature space clusters over the  
181 course of seizures, we employed a modified version of the  $L_{ratio}$  metric of cluster  
182 separation introduced and validated by Schmitzer-Torbert et al. (2005)<sup>58</sup> (see Methods).  
183 Cluster divisions with  $L_{ratio}$  less than 0.1 are considered to have a significantly low level  
184 of false negative contamination, indicating that drops in firing rate are not caused by  
185 over-assigning candidate spikes to noise or other clusters due to changing waveform  
186 shapes in these divisions. We consider units whose average contamination level across

187 seizure divisions (dynamic  $L_{ratio}$ ) is less than 0.1 to be a best-isolated subset<sup>58</sup>. Figure 2  
188 shows an example of an FS unit whose waveform shape could be well isolated from  
189 noise across the entire seizure despite showing a monotonic decrease in spike  
190 amplitude (Fig. 2a-c). The isolation quality of this unit throughout the seizure is  
191 demonstrated visually by 2D voltage histograms of these waveforms (Fig. 2d) and is  
192 quantitatively captured by its dynamic  $L_{ratio}$  being far below threshold in all seizure  
193 divisions in which it was active (Fig. 2b). This isolation quality was similarly sustainable  
194 throughout the seizure for many RS units (e.g. Extended Data Fig. 5), although at a  
195 lower proportion than FS units, with 48.6% of FS units meeting this criterion but only  
196 19.8% of RS units. This pattern sustained throughout seizures, with the proportion of  
197 well-isolated FS units remaining between 30% and 48% across all 8 seizure divisions  
198 and that of RS units remaining between 13% and 19% (Extended Data Fig. 6). The  
199 apparent difference in sortability by cell type may be because the frequency content of  
200 noise is such that random threshold crossings are more similar in shape and amplitude  
201 to the wider waveforms of RS units than to the sharper waveforms of FS units. This  
202 suggests that FS cell spikes are inherently more distinguishable from noise in human  
203 neocortical recordings even during seizures. We considered the best-isolated subset of  
204 units following this quantitative criterion in parallel with all-inclusive analyses of firing  
205 rate dynamics in various time divisions of seizures with similar results. In particular,  
206 similar temporal profiles by cell type were observed throughout seizures when  
207 considering all units or only best-sorted units with an average  $L_{ratio} < 0.1$  across all  
208 divisions for Patient C (Fig. 2e&f), as well as when comparing average firing rate time  
209 courses by cell type across all patients (Fig. 2g&h). Furthermore, the observed time

210 difference between mean RS activity cessation timing and mean FS activity cessation  
211 timing remained significantly larger than that expected by random cell-type label  
212 reshuffling when considering all units ( $p < 0.0001$ ; Fig. 2i), as well as only best-isolated  
213 units with maximum  $L_{ratio} < 0.1$  ( $p < 0.005$ ; Fig. 2j). Thus, FS cell cessation occurs several  
214 seconds before RS cell cessation across the population as well as for the very best  
215 isolated units.

216

217 The firing profile of individual FS cells and the accompanying changes in the seizure  
218 LFP amplitude were remarkably consistent across all secondary generalized focal  
219 seizures examined, independent of etiology or focus (Figs. 1, 2, and Extended Data  
220 Figs. 2-4). In patients with an etiology of mesial temporal sclerosis, where the seizure  
221 started focally in the hippocampus or surrounding medial temporal regions, FS cells in  
222 the temporal neocortex consistently stopped firing after the seizure secondarily  
223 generalized and spread to the neocortex, leading to accompanying increases in seizure  
224 LFP amplitude (Fig. 1a&b). Similarly, in a patient with an etiology of neocortical  
225 dysplasia (Patient C) where the seizure originated in the temporal neocortex, several  
226 cm from the implanted electrode array, FS cells near the array stopped firing within the  
227 first 40 seconds of the seizure spreading to that location (Fig. 2a&b). Again, this  
228 coincided with a transition to even larger amplitude spike-wave LFP events.

229

230 The variability in FS cessation times raises the question of how seizure waves travel  
231 across the neocortex: is there a wave that slowly moves across the cortex<sup>32</sup> or a series  
232 of faster waves that are perhaps altered by the local activity of FS cells<sup>11,30,33</sup>? We found

233 fast traveling LFP waves in all patients that swept across the 4x4 mm microelectrode  
234 array within 40 ms, at a speed of ~0.1 m/s, consistent with estimates from slice and  
235 computational studies<sup>30,34–36</sup>. There was a dramatic effect of individual FS cell activity:  
236 when an FS cell was still firing, it was able to impede and alter epileptic traveling waves  
237 (Fig. 3a), preventing the wave from increasing the seizure's LFP amplitude in the vicinity  
238 of the FS cell. Once the FS cell activity ceased, traveling waves swept through the  
239 entire array, successfully recruiting the area around the now-silent FS cell (Figure 3B).  
240 Indeed, once all FS cells had switched off, the path of epileptic traveling waves became  
241 far more regular and stereotyped. Thus, human FS inhibitory cells possess a  
242 remarkable capability to obstruct and alter the path of epileptic traveling waves. This  
243 again points to the importance of FS activity in controlling local neuronal activity and  
244 LFP dynamics during local seizure propagation but leaves open the question of what is  
245 causing them to stop firing during the seizure.

246  
247 There are two ways in which FS cells can stop firing during a seizure: 1) they could be  
248 hyperpolarized by inhibition from other inhibitory neurons<sup>22</sup>, also known as the  
249 disinhibition hypothesis<sup>23</sup>; or 2) they could enter depolarization block and thus become  
250 incapable of firing additional action potentials, despite receiving strong excitatory  
251 synaptic input<sup>12,14,25,56</sup>. These two scenarios produce very different predictions for how  
252 the action potential (AP) amplitude of an FS cell should change during a seizure. In the  
253 case of hyperpolarization, the AP amplitude should increase as the firing rate is  
254 decreasing. In the case of depolarization block, AP amplitude should decrease before  
255 the cell stops firing while its firing rate is also decreasing. To monitor the relative

256 contributions of hyperpolarization and excessive depolarization throughout the seizure  
257 in each recorded unit, we therefore devised a novel method that decodes the  
258 membrane potential regime of neurons from extracellular spike amplitude data by  
259 computing the sign of the correlation between AP amplitude and firing rate in each  
260 second of the seizure (Fig. 4a-c; see Methods). Some units first paused their firing due  
261 to transient inhibition from other cells, as suggested by strongly negative correlations  
262 between AP amplitude and firing rate as firing rate initially decreased (Fig. 4b&h;  
263 Extended Data Figs. 7&8). This period corresponded precisely to the time period of  
264 increased firing in neighboring FS units (Fig. 4d&j). However, these apparently  
265 hyperpolarized units resumed their firing after this pause. Cessation of firing  
266 subsequently occurred presumably due to massive depolarization of their membrane  
267 potential, as demonstrated by strongly positive correlations of AP amplitude and firing  
268 rate as these units stopped firing spikes (Fig. 4b&h). The regimes of negative  
269 correlation correspond to a dynamic inhibitory control of local firing rates during the  
270 seizure, followed by a regime of positive correlation with decreasing AP amplitudes  
271 during the final descent in firing rate, a pattern consistent with what is seen during  
272 depolarization block.

273  
274 This pattern was also seen on the population level in spiking event-triggered averages  
275 of the time course of our predicted membrane potential measure (Fig. 4e). Aligning  
276 inferred membrane potential time courses around the time of firing rate pauses  
277 (dropping below 30% of peak rate) revealed a large negative deflection for FS cells,  
278 indicative of these units being inhibited via hyperpolarization to reduce firing rate at this

279 time (Fig. 4e; n=12;  $R_{\text{mean,pause}}=-0.44\pm0.19$  [sem]; less than 0 with  $p<10^{-7}$  by bootstrap  
280 mean resampling test,  $n_{\text{sample}}=10$ ,  $N_{\text{bootstrap}}=50,000$ ). Furthermore, the inferred  
281 membrane potential amongst the FS cell population showed that this shift was also  
282 widespread (Fig. 4f), with 9 out of 12 (75%) FS units pausing during the negative,  
283 hyperpolarized regime during this rate-based event. Aligning inferred membrane  
284 potential time courses around the later time of firing rate cessation in units (defined by  
285 rate falling below 30% of peak rate for the final time) revealed a large positive deflection  
286 for FS cells, indicative of these units entering a regime depolarization block (Fig. 4e;  
287 n=26;  $R_{\text{mean,cess}}=+0.45\pm0.12$  [sem]; greater than 0 with  $p<10^{-7}$  by bootstrap mean  
288 resampling test,  $n_{\text{sample}}=20$ ,  $N_{\text{bootstrap}}=50,000$ ). Again, the inferred membrane potential  
289 amongst the FS cell population showed that this shift was also widespread across units  
290 (Fig. 4f), with 20 out of 26 (77%) FS units landing in the positive, over-excited regime.  
291 When comparing these values only in units that showed both a pause and cessation to  
292 control of heterogeneity amongst different units, the inferred membrane potential was  
293 still significantly higher as the unit ceased firing compared to as the unit paused its firing  
294 (right-sided Wilcoxon signed rank test; n=12, p=0.0049). Finally, these firing rate  
295 descents in FS cell activity were associated with distinct changes in LFP amplitude  
296 despite being of the same magnitude (at 30% of peak firing rate) as shown by event-  
297 triggered averages in LFP amplitude (Fig. 4e). FS cessation was associated with a  
298 larger LFP amplitude than that associated with pausing even amongst cells exhibiting  
299 both events (right-sided Wilcoxon signed rank test; n=12,  $p<10^{-4}$ ). Similar results were  
300 obtained indicative of significant and widespread overexcitation underlying the cessation  
301 of activity in RS units, with 225 out of 331 (68%) RS units with sufficient rate at the time

302 of cessation exhibiting a positive value (Extended Data Fig. 7e; n=331;  
303  $R_{mean,cess}=0.30\pm0.03$  [sem]; greater than 0 with  $p<10^{-7}$  by bootstrap mean resampling  
304 test,  $n_{sample}=20$ ,  $N_{bootstrap}=50,000$ ). However, amongst RS cells exhibiting a pause in  
305 activity, membrane potential appeared much more heterogenous despite controlling for  
306 firing rate at this time, appearing in a bimodal distribution amongst both inhibition and  
307 depolarization block that was not significantly different from 0 (Extended Data Fig. 7e&f;  
308  $n=130$ ;  $R_{mean,cess}=-0.08\pm0.06$  [sem]; greater than 0 with  $p=0.3782$ ,  $n_{sample}=10$ ,  
309  $N_{bootstrap}=50,000$ ). This may be because RS cells receive a greater diversity of input  
310 magnitudes during seizure progression than do FS cells but succumb to the same, more  
311 uniform mechanism underlying depolarization block at firing rate cessation and seizure  
312 transition, which we hypothesize is due to increasing potassium concentrations in the  
313 extracellular environment shared by all of these cells.

314  
315 This sequence of significant hyperpolarization in FS cells followed by large and  
316 widespread overexcitation in all cells suggests a consistent membrane potential-based  
317 mechanism by which local cortical circuits fight but ultimately succumb to seizure  
318 progression. The dynamics in firing rate and action potential amplitude that characterize  
319 this mechanism were accurately reproduced in a computational model of the cell  
320 membrane incorporating voltage-dependent sodium and potassium conductances  
321 (Hodgkin-Huxley formalism) with stochastic background synaptic input. The model  
322 reproduced all of the observed mutual dynamics between action potential rate and  
323 amplitude during inhibitory (hyperpolarizing) pauses versus depolarization-induced

324 cessation (Fig. 5), confirming the plausibility of this mechanistic sequence driving unit

325 activity patterns during seizure progression.

326

327

328 **DISCUSSION**

329 We have shown that both FS and RS cells are strongly activated during the initial  
330 spread of secondarily generalized seizures. The immediate increase in RS rate at  
331 seizure onset, in particular, clearly indicates spread of the seizure, and not a failed  
332 seizure in what has been called an ictal penumbra, where no initial increases in RS rate  
333 appear<sup>32</sup>. Importantly, we have shown that both FS and RS cells can sometimes pause  
334 their activity due to hyperpolarization (likely due to inhibition-mediated hyperpolarization  
335 from other nearby inhibitory neurons) but stop firing midway through secondarily  
336 generalized seizures due to depolarization block. This result is independent of seizure  
337 etiology (cortical dysplasia vs. mesial temporal sclerosis) or site of origin (hippocampus  
338 vs. neocortex). This suggests that there is an almost complete lack of FS-mediated  
339 inhibition towards the end of a human seizure, in contrast to some animal models  
340 without loss of inhibition<sup>18</sup>. FS cells are active near the beginning and middle of the  
341 seizure, in contrast to computational models placing the loss of inhibitory restraint at  
342 seizure onset<sup>37</sup>. Strikingly, this absence of FS inhibitory activity is accompanied by large  
343 increases in the amplitude of the seizure's LFP and unimpeded fast traveling waves, as  
344 well as a short-lasting increase in RS firing. Thus, these results suggest a more  
345 complicated set of dynamics than a monotonic increase or decrease of inhibition and  
346 provide further insight into the associated biophysical mechanisms.

347

348 The main difference between RS and FS cell firing during the seizures observed here  
349 was the significantly earlier cessation of spiking by FS cells, which is consistent with  
350 previous results from *in vitro* models of seizure-like events showing increased

351 propensity of FS cells to enter depolarization block compared to pyramidal cells<sup>12,14,25</sup>.  
352 The reason for this difference in propensity to enter depolarization block has not been  
353 established, but these results suggest this difference could represent a primary source  
354 of imbalance between excitatory and inhibitory cell activities that allows seizures to  
355 propagate and transition to a large amplitude phase in human neocortex. One  
356 hypothesis accounting for this difference is that of the differential expression of voltage-  
357 gated potassium channel units in FS as opposed to RS cells<sup>38–40</sup> in combination with the  
358 elevated extracellular potassium ion levels known to occur in the context of  
359 seizures<sup>41,42</sup>. However, there are several intrinsic and network-based properties that are  
360 known to differ between FS cells and pyramidal cells and could contribute to this  
361 difference, such as intrinsic excitability and the relative strength of feedforward drive<sup>43–</sup>  
362 <sup>46</sup>. The results here suggest that properties responsible for increasing the propensity of  
363 FS cells to enter depolarization block relative to RS cells are also those that allow the  
364 propagation and exacerbation of seizures in human neocortex. Beyond seizure  
365 progression, it is also possible that the lack of FS activity sets in motion a critical  
366 network-level transition that leads to seizure termination<sup>47–49</sup>. This transition may include  
367 the activation of inhibitory cell types other than FS cells<sup>22,59</sup>.

368

369 In summary, FS cells are the largest source of inhibition in the neocortex, and human  
370 FS cells approach cessation less than halfway through a seizure, most likely due to  
371 depolarization block. This is associated with a dramatic increase of the seizure's local  
372 field potential amplitude and a transition to clear spike-and-wave events at a frequency  
373 of ~3 Hz. Rhythmic spike-and-wave discharges, when they occur in the motor cortex,

374 are responsible for the rhythmic ~3 Hz movements seen during the clonic phase of  
375 tonic-clonic seizures<sup>50</sup>. Importantly, this suggests a novel, FS-dependent, mechanistic  
376 explanation for the two behaviorally defined phases of secondarily generalized tonic-  
377 clonic seizures: the high-FS-rate, low-LFP-amplitude phase of the seizure corresponds  
378 to the tonic phase, whereas the post-FS-cessation phase with periodic spike-wave  
379 bursts corresponds to a longer lasting clonic phase. Thus, in addition to existing  
380 approaches<sup>51-55</sup>, novel therapies that prevent FS cells from entering depolarization  
381 block may prevent - or at least limit the severity of - seizures, representing a novel and  
382 potentially powerful avenue for treating seizures with many different etiologies.

383

384

385 **METHODS**

386 **Patients & Clinical/Research Electrode Placement**

387 Approval for all experiments was granted by the Institutional Review Boards of  
388 Massachusetts General Hospital / Brigham & Women's Hospital and Rhode Island  
389 Hospital. The decision to implant intracranial electrodes in an epilepsy patient as well  
390 the positioning of those electrodes in a patient was made solely on clinical factors by  
391 clinical staff. The explicit goal of this study was to examine the single neuron correlates  
392 of tonic-clonic seizures<sup>42</sup> with focal onsets (also referred to as focal seizures with  
393 secondary generalization), one of the most common kind of epilepsies<sup>56</sup>. These focal  
394 seizures have a localized onset zone, either in the mesial temporal lobe or neocortex,  
395 but secondarily generalize, spreading to both hemispheres and almost always leading  
396 to impaired consciousness. Here, we studied data from 4 patients (Patients A,B,C,D)  
397 with clear focal seizures with secondary generalization, with each of these clinical  
398 seizures showing clear spike-and-wave patterns. Two additional patients with temporal-  
399 lobe epilepsy were implanted with NeuroPort Arrays but not studied here because one  
400 of them did not have any seizures while implanted (Patient E), and the NeuroPort Array  
401 in the other patient did not sample any typical spike-and-wave seizures (Patient F). A  
402 total of 10 secondarily generalized seizures with spike-and-wave discharges from the 4  
403 patients were analyzed (3 each from Patients A and D; 2 each from Patients B and C).  
404 A detailed clinical description of each of these 4 patients follows:  
405 **Patient A.** Patient A was a left-handed man in his 30s at the time of his surgery. He had  
406 suffered from pharmacologically intractable partial complex seizures for almost two  
407 decades. His seizures lasted 1-2 minutes and were characterized by a sudden onset of

408 slurred and nonsensical speech. This was followed by a staring spell, lack of  
409 responsiveness, and head turning to the right. He also displayed automatisms and  
410 posturing that involved his right arm and hand more than his left. MRI suggested left  
411 (dominant) temporal polymicrogyria. He underwent placement of grids and strips for ~2  
412 weeks to delineate the seizure focus with respect to this area of abnormal sulcation. A  
413 4x4 mm NeuroPort array with 1.5 mm long contacts was placed in the left superior  
414 temporal gyrus. Seizures were found to emanate from the mesial temporal structures,  
415 but during secondary generalization, the seizures spread to the location of the array in  
416 the superior temporal gyrus and beyond. The patient underwent a left temporal  
417 lobectomy, and histology confirmed that the microarray targeted layer 3. Pathology was  
418 consistent with mesial temporal sclerosis.

419

420 **Patient B.** Patient B was a right-handed man in his 40s at the time of his surgery, with a  
421 history of medically refractory epilepsy. His seizures lasted 1-2 minutes. Clinically, the  
422 seizures started with arousal and bilateral arm and leg extension. This was followed by  
423 leftward head deviation, left arm flexion, and generalized tonic-clonic activity. He  
424 underwent placement of grids, strips, and depths in his right hemisphere. A 4x4 mm  
425 NeuroPort array (with 1.5 mm deep contacts) was placed in the right middle temporal  
426 gyrus. During secondary generalization, the seizures spread to the location of the  
427 NeuroPort array in the middle temporal gyrus and beyond. The patient underwent a  
428 right temporal lobectomy. Histology on the resected tissue confirmed that the microarray  
429 targeted layer 3.

430

431 **Patient C.** Patient C was a left-handed woman in her 20s at the time of her surgery.  
432 She started to have complex partial seizures at least 10 years prior to surgery. These  
433 seizures included an aura of nausea and a ‘tunneling’ sensation, then a flattening of  
434 affect, slowed responsiveness, automatisms, and associated amnesia. Such seizures  
435 occurred 3-4 times per month and were persistent despite being on a three-drug  
436 anticonvulsant regimen. MRI revealed an extensive nodular gray matter heterotopia in  
437 the right hemisphere. Video-EEG monitoring had found right hemispheric onset  
438 seizures, and fMRI had shown normal left sided language activation patterns and  
439 normal motor activation patterns. Wada testing confirmed left hemispheric language  
440 dominance and suggested her left hemisphere could adequately support memory  
441 function subsequent to a right temporal lobectomy. Based on these data, she was  
442 implanted with a combination of subdural grid and strip electrodes over the right  
443 hemisphere and 3 depth electrodes into the right temporal lobe. The NeuroPort array  
444 (with 1.5 mm deep contacts) was placed in the right middle temporal gyrus. Her  
445 seizures lasted between 1-2.5 minutes. These showed very consistent patterns of  
446 seizure onset and propagation on ECoG; all began in the right middle and upper gyri of  
447 the posterior temporal cortex. Low amplitude and fast activity were recorded from these  
448 grid sites at the onset, followed by a buildup of 11-13 Hz activities from these leads  
449 which then spread anteriorly and inferiorly along the grid. Rhythmic spike-wave  
450 discharges were also detected soon after seizure onset spreading to several locations,  
451 including the location of the NeuroPort array in the right middle temporal gyrus. The  
452 patient underwent an extensive right temporal resection with extension posteriorly  
453 toward the right temporo-occipital junction but sparing of much of the mesial temporal

454 structures (including the hippocampus). Histology confirmed that the array targeted  
455 layers 2/3. Pathology revealed subtle neuronal dysgenesis and focal superficial gliosis  
456 and encephalomalacia in the posterior temporal neocortex, including the recorded  
457 seizure-onset zone. Anterior temporal cortex showed mild gliosis.

458

459 **Patient D.** Patient D was a right-handed man in his 20s whose seizures began when he  
460 was a teenager. His seizures were characterized by a blank stare and oral automatisms  
461 accompanied by stiffening and posturing of the right hand. His MRI was unremarkable,  
462 but his semiology and phase I EEG recordings suggested a left temporal seizure onset.  
463 Consequently, he was implanted with several strip electrodes covering the left frontal  
464 and temporal regions. The NeuroPort array (1.0 mm deep contacts) was placed in the  
465 middle temporal gyrus about 1–2 cm posterior to the temporal tip. All of the seizures  
466 had similar clinical and electrographic signatures with a left gaze preference at onset  
467 followed by tonic and then clonic movements of the right arm. Electrographically, the  
468 seizures began with a generalized burst of sharp waves followed by sharp wave com-  
469 plexes that were maximal in mesial temporal leads. The participant underwent a left  
470 temporal lobectomy. Histological examination of the tissue revealed mild dysplastic  
471 changes in the lateral temporal neocortex and gliosis and moderate neuronal loss in  
472 regions CA4 and CA3 of the hippocampus.

473

#### 474 **NeuroPort Recordings, Data Collection & Analysis**

475 A Neuroport array (manufactured by Blackrock Microsystems) is a 10x10 grid of  
476 electrodes with an inter-electrode spacing of 400 um, giving a total size of 4x4 mm. The

477 depth of the electrodes used in this study was either 1.5 mm (Patients A,B,C) or 1.0 mm  
478 (Patient D). 96 of the 100 electrodes were used to record the activity of individual  
479 neurons as well as the local field potential (LFP). The 0.3-7500 Hz wideband analog  
480 signal from each electrode was referenced to a distant intracranial reference wire and  
481 sampled at 30 kHz. The LFP shown in Figs. 1, 2, and Extended Data Fig. 1 were z-  
482 scored, but not filtered any further. Traveling wave analysis & images (Fig. 3) made use  
483 of these z-scored, unfiltered LFP signals. For single unit analysis, the broadband signal  
484 was high-pass filtered above 250 Hz using a 6-pole Bessel filter and then manually  
485 spike-sorted using Plexon Offline Sorter. We then classified the neurons as either fast-  
486 spiking (FS) inhibitory interneurons or regular-spiking (RS) excitatory cells using well-  
487 established criteria<sup>27,28</sup>, including action potential shape. Cessation of firing during a  
488 seizure was defined as the bin after which the firing rate never exceeded 30% of the  
489 unit's peak rate. For action-potential (AP) amplitude analysis (Fig. 4a), the AP amplitude  
490 was defined as the trough-to-peak amplitude of each individual extracellular action  
491 potential.

492

#### 493 **Cluster isolation quality assessment: Dynamic L<sub>Ratio</sub>**

494 To assess the isolation quality of feature space clusters over the course of seizures, we  
495 employed a modified version of the L<sub>ratio</sub> metric of cluster separation introduced and  
496 validated by Schmitzer-Torbert et al. (2005)<sup>58</sup>. This involved first calculating the  
497 Mahalanobis distance of every spike to a given cluster's center in a 4D feature space  
498 consisting of trough-to-peak amplitude, trough-to-peak width, principal component 1,  
499 and principal component 2. The Mahalanobis distance normalizes the Euclidean

500 distance by the variance of a given cluster along its major dimensions to correct for  
501 correlations amongst features. Schmitzer-Torbert et al. (2005)<sup>58</sup> showed strong error  
502 rate correlation with ground truth extracellular spikes by assuming a multi-dimensional  
503 Gaussian distribution for a given cluster and taking the amount of contamination by  
504 false negative assignments to be the sum of probabilities of each un-clustered spike of  
505 a given Mahalanobis distance to belong to that Gaussian, which was robust to the  
506 particular feature space used. These probabilities are given by the inverse of the  
507 cumulative distribution function of a chi-squared distribution with degrees of freedom  
508 equal to the number of features in the features space, the sum of which is called L.  
509 Because clusters in this space moved over the course of the seizure in a non-monotonic  
510 pattern here, we calculated Mahalanobis distances to a surrogate cluster for multiple  
511 subsets of the whole cluster at 8 equal divisions over the course of the seizure and 3  
512 divisions of the 10 minute period that occurred two minutes after the end of the seizure.  
513 A composite cluster across initial divisions was used to provide a liberal estimate of the  
514 space that a given cluster might occupy despite early waveform shape changes. This  
515 composite reference cluster included all available spikes before the seizure along with  
516 those in the first two divisions of the seizure, which were generally well-sortable. We  
517 calculated the sum of false negative assignment probabilities under a Gaussian model  
518 for this reference cluster, the value L, for each seizure and post-seizure division. We  
519 then dynamically normalized L by the number of spikes assigned to the cluster in each  
520 time division to estimate contamination rates relative to the number of spikes assigned  
521 during that division, which we refer to as the dynamic L<sub>ratio</sub>.

522

523 **Membrane potential trajectory analysis**

524 We exploited the biophysical relationship between depolarization, voltage-gated Na<sup>+</sup>  
525 channel inactivation, and spike waveform shape<sup>60</sup> to infer the direction of membrane  
526 potential changes underlying the changes in firing rate exhibited by single units  
527 recorded extracellularly in patients across time. This was done for a given unit by first  
528 computing the local spike rate and average trough-to-peak waveform amplitude in  
529 moving time windows of width 1 second unless otherwise specified, moving with a step  
530 size of 0.1 seconds. Then a linear regression was performed at each point in this series  
531 across a moving time window of 3 seconds, producing a time series of correlation  
532 coefficients for bins with an average spike rate of at least 5 Hz. Strong negative  
533 correlations were taken as evidence of firing rate changes associated with membrane  
534 potential changes near resting membrane potential, while strong positive correlations  
535 were taken as evidence of membrane potential changes closer to firing threshold, near  
536 the regime of depolarization block<sup>56</sup>.

537

538 **Computational model**

539 Computer simulations of transmembrane voltage dynamics consistent with the  
540 extracellular observations here were made in MATLAB R2017b to explore plausible  
541 underlying biophysical mechanisms. A 4-dimensional ordinary differential equation  
542 model of a patch of neural membrane following the Hodgkin-Huxley formalism of  
543 passive ( $g_L=0.033 \text{ mS/cm}^2$ ,  $E_L=-60 \text{ mV}$ ,  $I_L=g_L(V-E_L)$ ) and voltage-dependent spiking Na<sup>+</sup>  
544 ( $g_{Na}=60.0 \text{ mS/cm}^2$ ,  $E_{Na}=+58 \text{ mV}$ ,  $I_{Na}=g_{Na}m^3h(V-E_{Na})$ ) and K<sup>+</sup> ( $g_K=5 \text{ mS/cm}^2$ ,  $E_K=-85$   
545 mV,  $I_K=g_Kn^4(V-E_K)$ ) conductances was solved using Euler integration with a timestep of

546 0.005 msec. First order kinetics of gating variables  $m$ ,  $h$ , and  $n$  were modeled as in  
547 previously established models of this form<sup>57</sup>. Slowly changing net synaptic input and  
548 extracellular ion gradient changes were considered to constitute a net external drive  
549 modeled as an injected inward current. This current follows a temporal form  
550 hypothesized to drive human neocortical neurons during secondarily generalized  
551 seizures based on the dynamic membrane potential decoding analysis performed here.  
552 Fast synaptic inputs were modeled as conductances with a maximum conductance  
553  $g_{syn}=0.15 \text{ mS/cm}^2$  and an exponential decay time course of 5 milliseconds gated by  
554 input spike times generated by a Poisson process with a linearly increasing rate  
555 parameter from 0.001 to 0.2 Hz representing increasing input firing rates across seizure.  
556 Analysis of the resulting spike trains was completed in the same manner as dynamic  
557 membrane potential trajectory decoding was performed for the observed extracellular  
558 data.

559

## 560 **Statistical analyses**

561 In performing hypothesis testing on various metrics describing activity amongst FS and  
562 RS units including peak firing rate difference, mean cessation time difference, and mean  
563 correlation between spike firing rate and action potential amplitude at time of cessation,  
564 we employed bootstrap-based methods to quantify the uncertainty in these metrics. For  
565 peak firing rate and cessation time differences this involved combining all relevant unit  
566 measurements into a single population, randomly reshuffling RS and FS labels amongst  
567 this population, and recomputing the relevant difference metrics  $N_{bootstrap}$  times as  
568 indicated to generate a distribution of the metric for random unit classifications. The

569 probability of a Type-I (false positive) error, the p-value, was then reported as the area  
570 under the distribution corresponding to values more extreme than the observed value  
571 for the original data. For testing the positivity of the mean correlation between spike  
572 firing rate and action potential amplitude at time of cessation, this involved first removing  
573 correlation coefficients in the time series corresponding to a linear regressions involving  
574 spike rates of less than 5 Hz. Then the coefficients at each unit's detected cessation  
575 time were resampled with replacement in 20 unit subpopulations 50,000 times (unless  
576 otherwise specified) and averaged to generate a bootstrapped sample mean distribution  
577 characterizing the variability in this mean relative to zero. The probability of a Type-I  
578 (false positive) error that the observed mean coefficient was greater than zero by  
579 chance, the p-value, was then reported as the area under the distribution corresponding  
580 to values equal to or less than zero. To nonparametrically test the significance of  
581 differences in paired measures at cessation and pause times within single units, we  
582 employed the right-sided Wilcoxon signed rank test (RMatlab2017b).

583

584 **Extended Data / Supplementary Information**

585 9 Extended Data Figures (+ legends) are included.

586

587

588

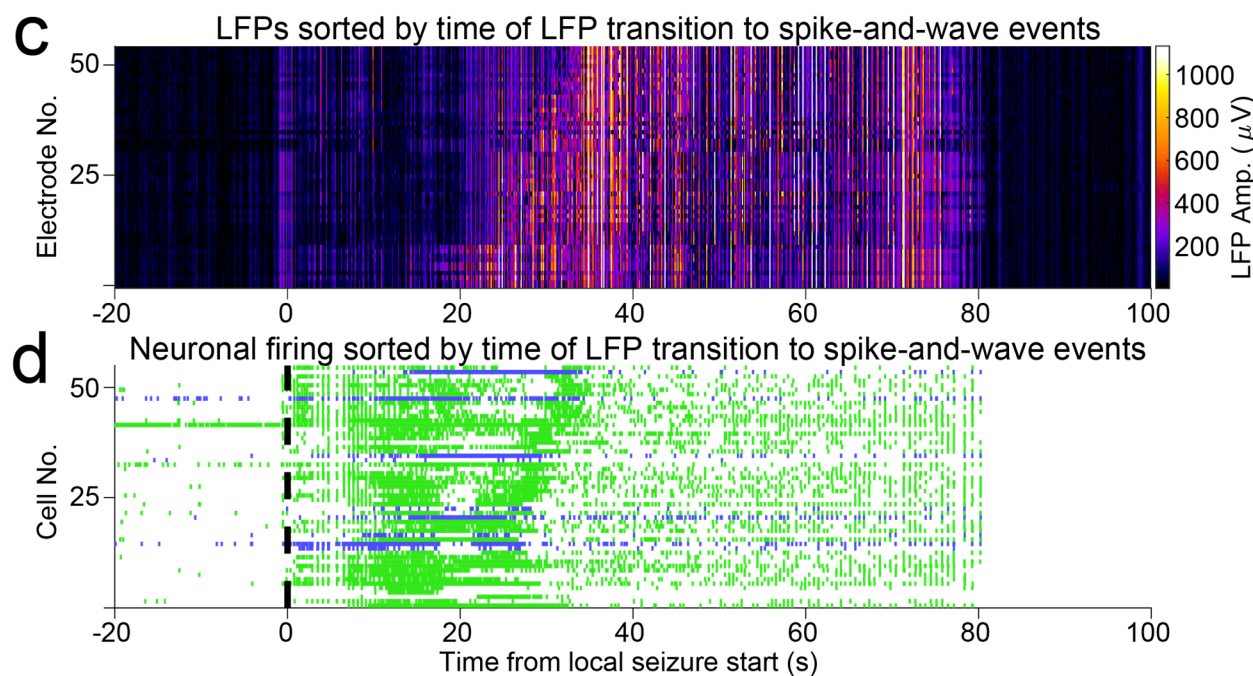
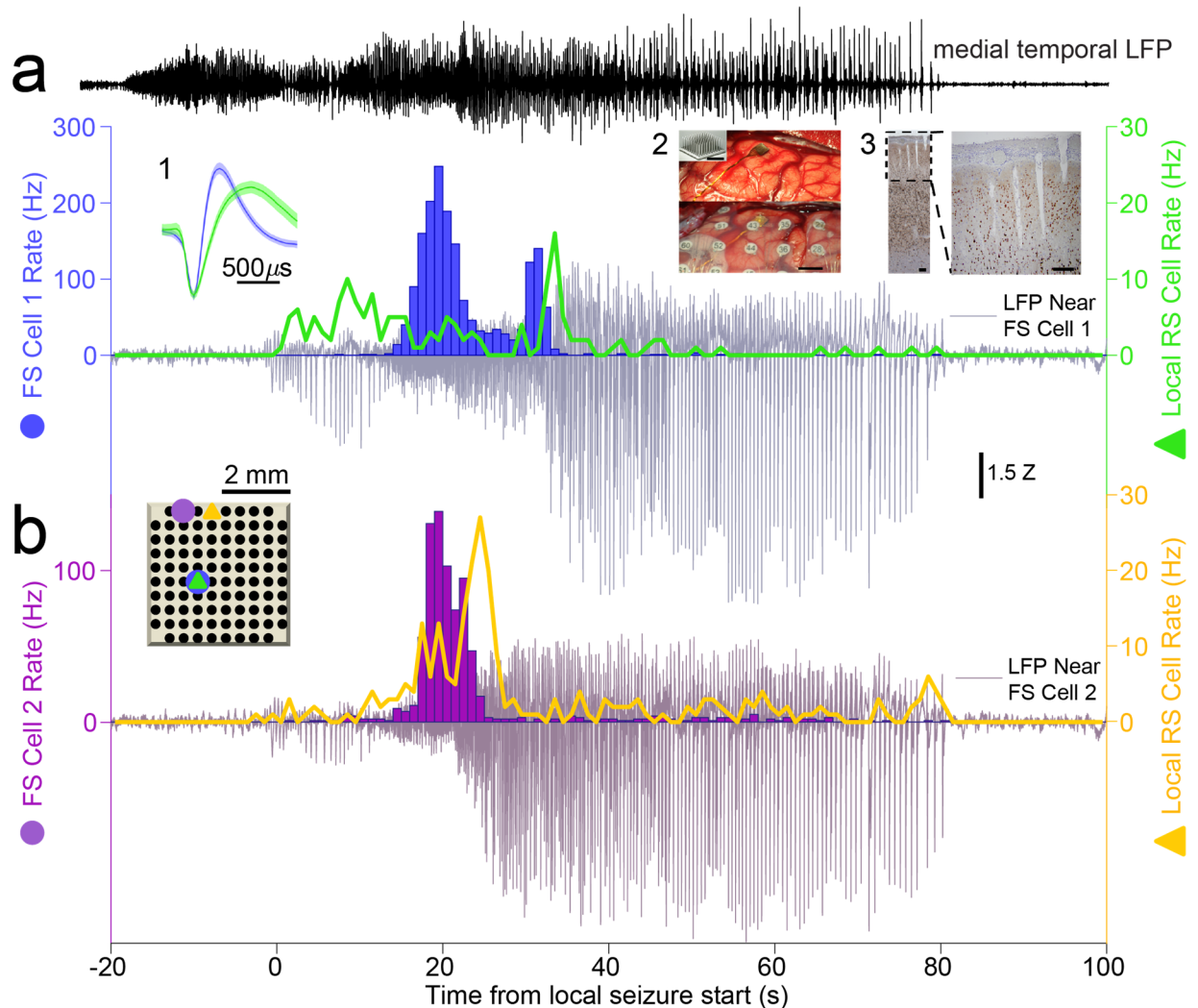
589 **ACKNOWLEDGEMENTS**

590

599 We would like to thank the patient volunteers. This work was supported by the American  
600 Epilepsy Society Junior Investigator Research Award, CURE Epilepsy Taking Flight  
601 Award, NINDS F32-NS083208 and University of Michigan Startup Funds (OJA), NIH  
602 R01-NS062092 (SSC) and NSF graduate student fellowships (TTJ & EKWB).

603

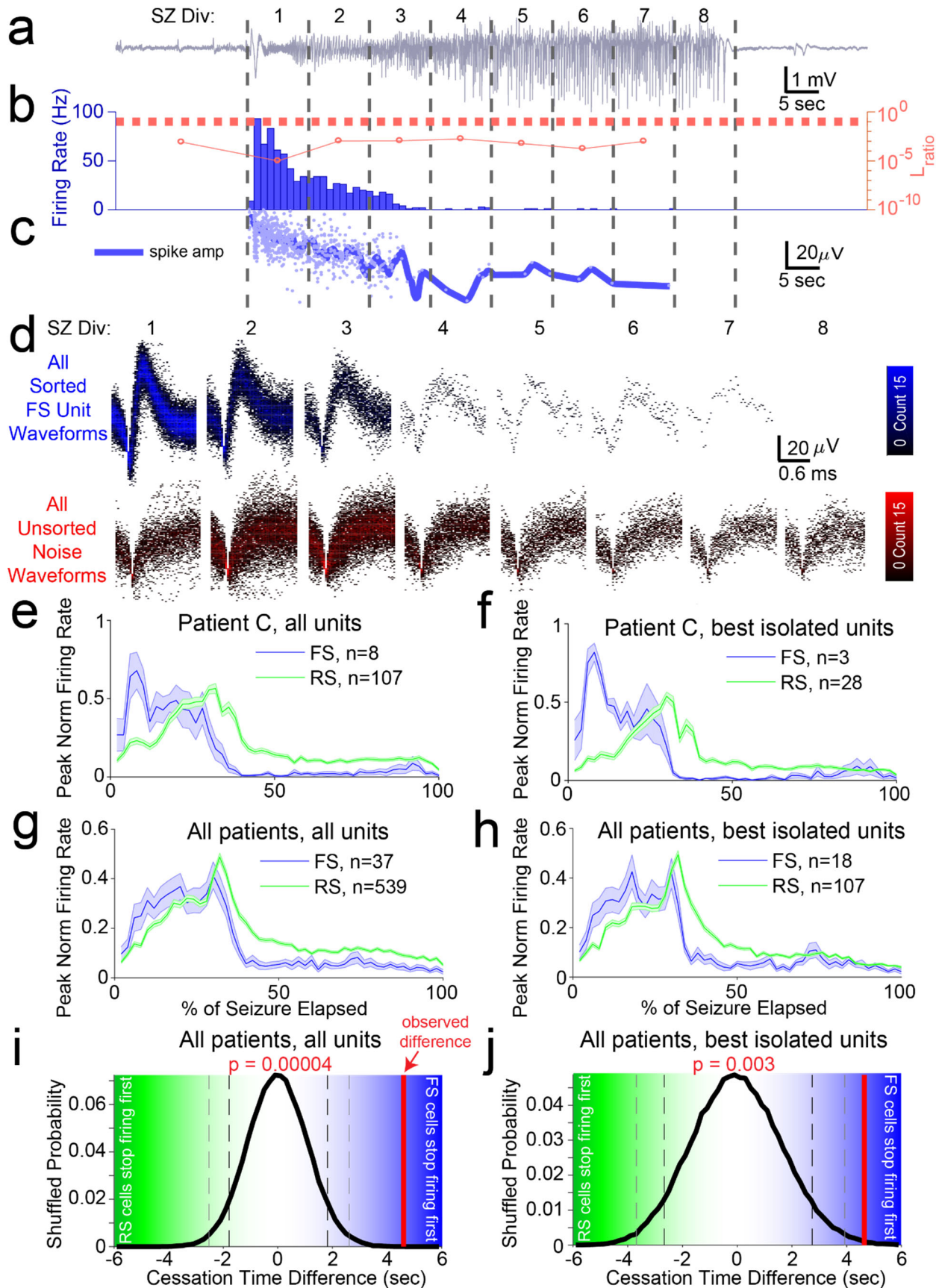
604 **FIGURES AND FIGURE LEGENDS**



606      **Figure 1: Human neocortical inhibitory and excitatory neurons have different temporal profiles**  
607      **relative to secondarily generalized focal seizure progression on local electrodes**  
608

- 609      a. **Upper.** Electrocorticogram trace (ECoG, black) from contact closest to source of focal seizure in  
610      hippocampus of Patient A. Note its time of initiation at T = -20 seconds, substantially preceding  
611      the start of the seizure in neocortex. **Lower.** The firing rate of a single FS cell (blue), the firing  
612      rate of a single RS cell recorded from the same electrode (green) and the local field potential  
613      (LFP, gray, recorded from the same electrode as the FS cell) during a seizure recorded from  
614      Patient A. Note the decrease in LFP amplitude as the FS cell starts firing, followed by a dramatic  
615      increase in LFP seizure amplitude after the FS cell decreases its rate at T=35 seconds. RS cell  
616      quickly increases its firing rate as the seizure first spreads to the NeuroPort array (T=0 seconds),  
617      then decreases in rate slightly as the FS cell switches on, and finally settles into a lower firing rate  
618      regime during the large spike-and-wave events that dominates the remainder of the seizure after  
619      FS cell cessation. Inset shows the mean normalized extracellular action potential waveforms (with  
620      99% confidence intervals in lighter shading) of FS Cell 1 (blue) and the neighboring RS cell  
621      (green). Inset 1: the mean normalized extracellular action potential waveforms (with 99%  
622      confidence intervals in lighter shading) of FS Cell 1 (blue) and the neighboring RS cell (green).  
623      Inset 2: The implanted microelectrode array (Top) with overlaid clinical grid electrodes (Bottom);  
624      Scale bar: 1 cm. Top left corner shows the array before implantation. Scale bar: 200  $\mu$ m. Inset 3:  
625      Histology of resected tissue showing the NeuN-stained neurons in the full neocortical column and  
626      electrode tracts and an enlarged image (Right) showing that the array targeted layer 3 of the  
627      neocortex. Scale bars: 400  $\mu$ m.  
628
- 629      b. The inset shows a schematic of the array and the location of two simultaneously recorded FS  
630      cells separated by ~2 mm: FS Cell 1 (blue, firing rate shown in Fig. 1c) and FS Cell 2 (purple). FS  
631      Cell 2 approached cessation at T=24 seconds, well before FS Cell 1. The LFP (grayish-purple)  
632      recorded at the same location as FS Cell 2 dramatically increases at the same time as FS Cell 2  
633      decreases firing, well before the increase seen in the LFP recorded next to FS Cell 1. These  
634      suggest the activity of FS cells during human seizures is strongly correlated to the local intensity  
635      of seizure waves. FS Cell 2 activity cessation again precedes a sharp increase in local RS cell  
636      activity (gold), further suggesting an important role of FS cells in controlling local activity during  
637      seizure progression.  
638
- 639      c. Heatmap shows local LFP amplitude (absolute value) over time on each electrode in NeuroPort  
640      array exhibiting classifiable units as each row, sorted by time of start of spike-and-wave event  
641      and with brighter colors indicating larger amplitudes. Note the increasing delay to start of spike-  
642      and-wave event suggesting different dynamics to seizure spread across the array over the  
643      timecourse of approximately 20 seconds.  
644
- 645      d. Raster plot showing spike times of all cells on NeuroPort array in Patient A that could be  
646      classified into FS (blue) or RS (green) categories with rows sorted by the same order as in (C).  
647      Note the increasing delay to reduction in spike density corresponding to LFP transition to spike-  
648      and-wave events suggesting control of local seizure progression by local cellular spiking activity.  
649

650



652      **Figure 2: Analyzing unit subpopulations by isolation quality demonstrates consistent cell-type**  
653      **specific activity profiles and cessation order despite changing unit amplitude and noise structure.**  
654

- 655      a. LFP in Patient C indicating seizure as split into 8 equal time divisions for analysis of unit isolation  
656      quality across duration of seizure.  
657
- 658      b. Bar graph shows firing rate in 1 second bins of best-isolated example FS unit (blue) in Patient C.  
659      Dotted red line indicates threshold used to determine best-isolated units using the dynamic  $L_{ratio}$   
660      measure (see Methods) in each time division of seizure. Line plot indicates dynamic  $L_{ratio}$  in each  
661      division (red) and shows large separation of example FS unit from noise in feature space used for  
662      clustering throughout the seizure (note log scale).  
663
- 664      c. Line plot showing average spike amplitude (dark blue) and individual spike amplitudes (light blue)  
665      of example FS unit over course of seizure in Patient C. Note that even as amplitude decreases  
666      the unit remains well-isolated from noise as quantified by dynamic  $L_{ratio}$  across seizure.  
667
- 668      d. Time-voltage histogram of all threshold crossings assigned to this example FS unit (blue, *Upper*)  
669      and to noise (red, *Lower*) in eight divisions of seizure in Patient C. Shows unit waveforms are  
670      visually distinguishable from threshold crossings assigned as noise across seizure.  
671
- 672      e. Average firing rate traces across seizures for each cell type group in Patient C, with y-axis  
673      normalized to firing rate peak and x-axis normalized to total seizure duration before averaging.  
674      Note right-shifted rate profile of RS units over course of seizure as compared to FS units.  
675
- 676      f. Average firing rate traces across seizures for each cell type group using only best-isolated units  
677      (see Methods) in Patient C, with y-axis normalized to firing rate peak and x-axis normalized to  
678      total seizure duration before averaging. Note right-shifted rate profile of best-isolated RS units  
679      over course of seizure as compared to best-isolated FS units.  
680
- 681      g. Average firing rate traces across seizures for each cell type group across all patients, with y-axis  
682      normalized to firing rate peak and x-axis normalized to total seizure duration before averaging.  
683      Note right-shifted rate profile of RS units over course of seizure as compared to FS units.  
684
- 685      h. Average firing rate traces across seizures for each cell type group using only best-isolated units  
686      (see Methods) across all patients, with y-axis normalized to firing rate peak and x-axis normalized  
687      to total seizure duration before averaging. Note right-shifted rate profile of best-isolated RS-  
688      classified units over course of seizure as compared to best-isolated FS-classified units.  
689
- 690      i. Observed time difference (solid red line) between mean RS activity cessation timing ( $n=399$ ) and  
691      mean FS activity cessation timing ( $n=37$ ) in relation to probability distribution of this timing  
692      difference across random label reshufflings of unit cell type labels ( $N_{shuffles}=100,000$ ; solid black  
693      line). P-value indicates probability of observing a value equal to or more extreme than the  
694      observed value simply by random assignment of cell type to each unit. Values on the right half  
695      correspond to a positive difference between RS and FS cessation, with larger values associated  
696      with increasing certainty that FS cells stop firing before RS cells. Values on the left half  
697      correspond to a negative difference between RS and FS cessation times, with larger values  
698      associated with increasing certainty that RS cells stop firing before FS cells.  
699
- 700      j. Observed time difference (solid red line) between mean best-isolated RS activity cessation timing  
701      ( $n=83$ ;  $Lratio < 0.1$  during middle 3 seizure divisions) and mean best-isolated FS activity  
702      cessation timing ( $n=17$ ;  $Lratio < 0.1$  during middle 3 seizure divisions) in relation to probability  
703      distribution of this timing difference across random label reshufflings of unit cell type labels  
704      ( $N_{shuffles}=100,000$ ; solid black line). P-value indicates probability of observing a value equal to or  
705      more extreme than the observed value simply by random assignment of cell type to each unit.  
706      Values on the right half correspond to a positive difference between best-isolated RS and best-  
707      isolated FS cessation times, with larger values associated with increasing certainty that best-

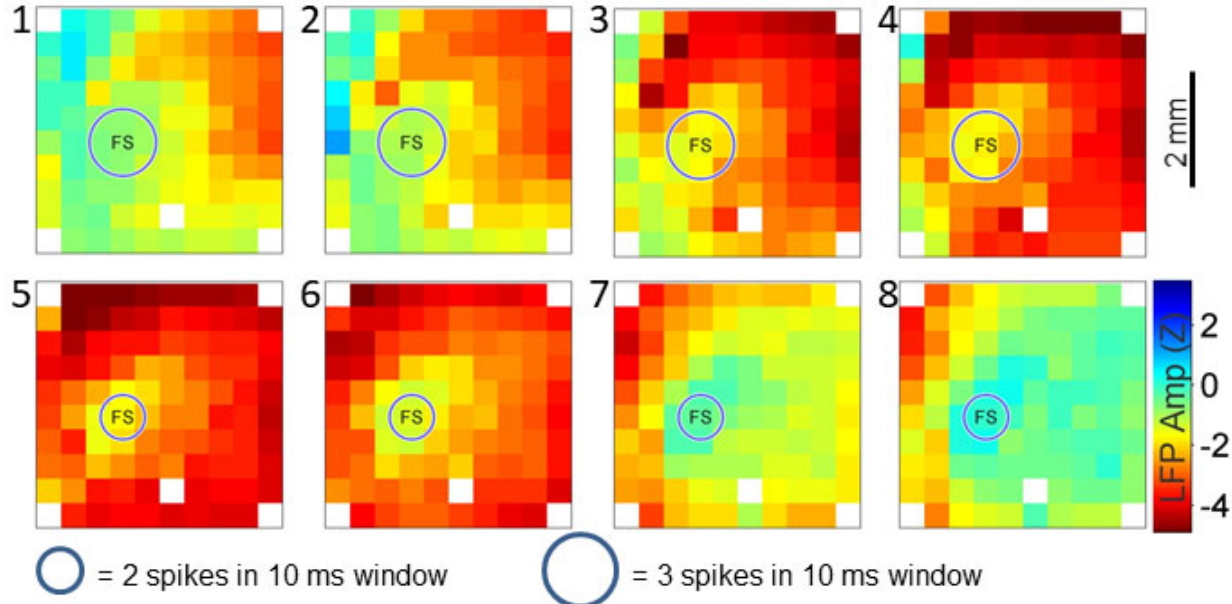
708 isolated FS cells stop firing before best-isolated RS cells. Values on the left half correspond to a  
709 negative difference between best-isolated RS and best-isolated FS cessation, with larger values  
710 associated with increasing certainty that best-isolated RS cells stop firing before best-isolated FS  
711 cells.

712

713

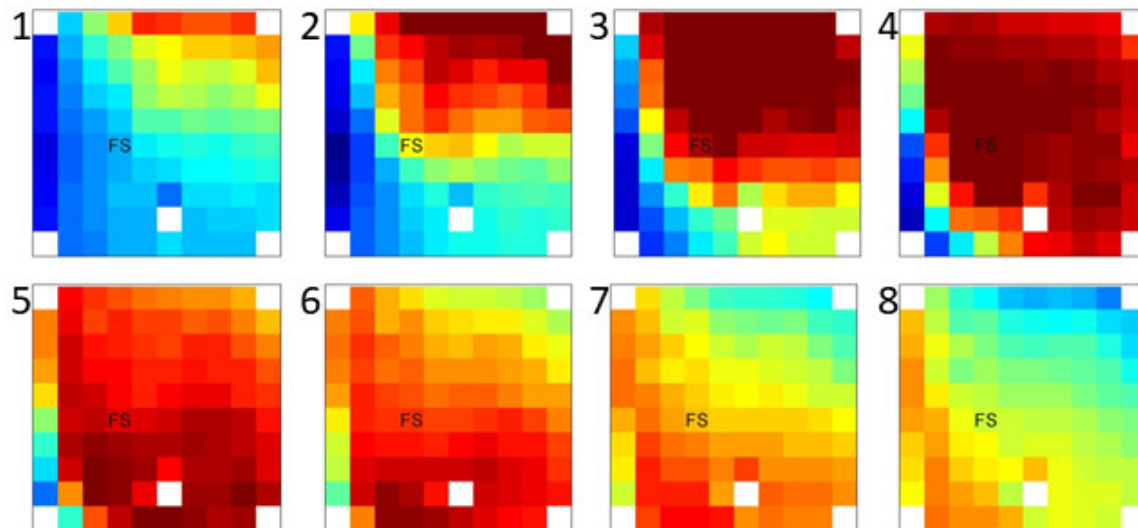
a

Epileptic traveling wave while FS cell is still firing



b

Epileptic traveling wave after FS cell has stopped firing



714

715

716

717

718

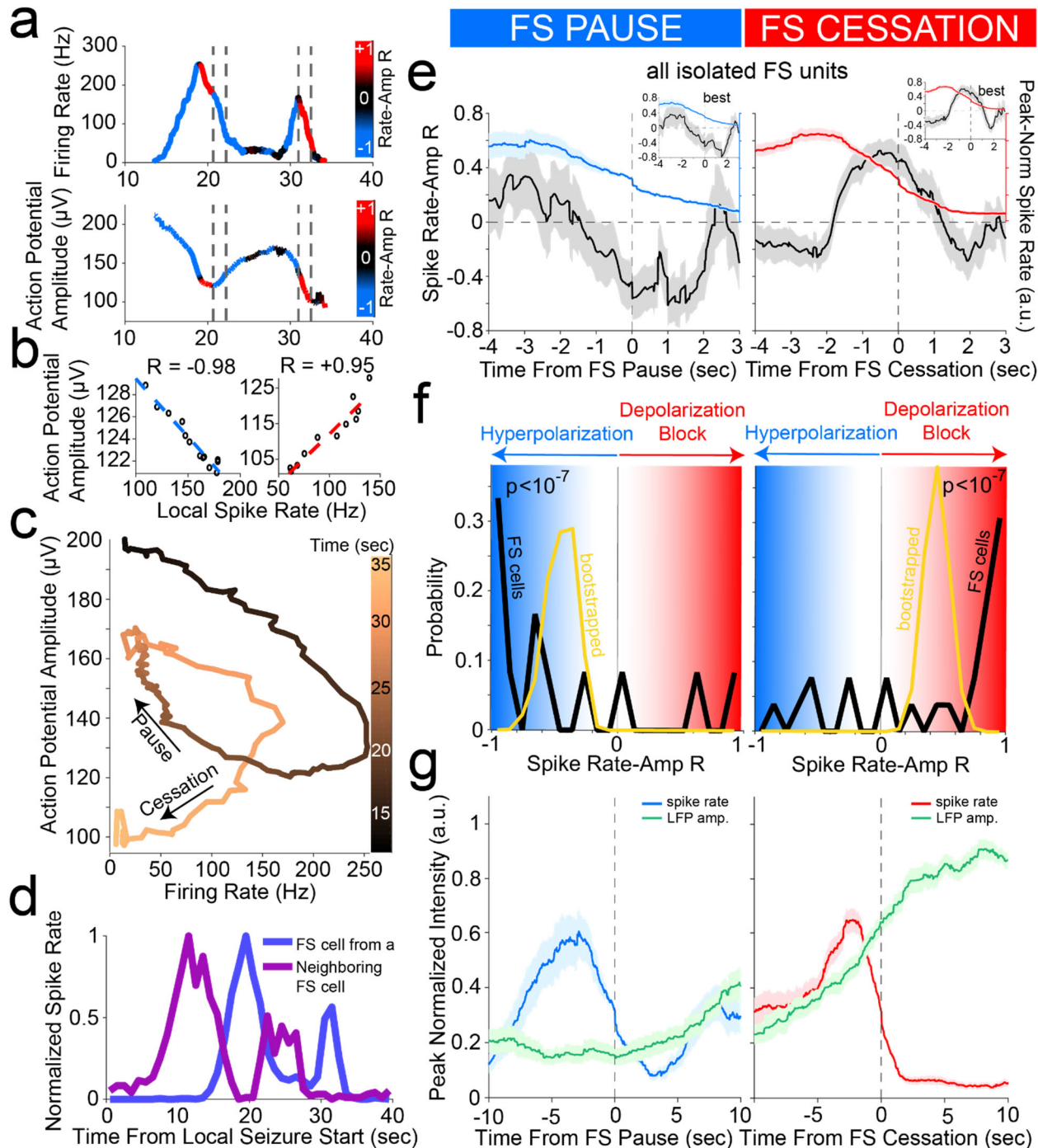
**Figure 3: Fast-spiking inhibitory neurons, when still firing, impede the spread of epileptic traveling waves.**

- 719        a. An example of a traveling wave recorded 30 seconds after the start of a seizure in Patient A. The  
720        FS cell located at the position marked “FS” was firing at high rates at this time. The 8 snapshots  
721        (1-8) are taken over a 35 ms interval as the traveling LFP wave starts in the top-right corner of the  
722        array and travels across the array. The traveling wave does not fully invade the region of  
723        neocortex containing the active FS cell, resulting in lower amplitude LFPs around the FS cell. In  
724        each subfigure, each square denotes a single LFP sensor, and white squares indicate omitted  
725        sensors.  
726  
727        b. An example of a traveling wave recorded 49 seconds after the start of the same seizure. In the  
728        absence of FS cell firing, the epileptic traveling wave moves unimpeded through the array, fully  
729        invading the region around the marked FS cell and resulting in larger amplitude LFPs at all  
730        locations.

731

732

733



734

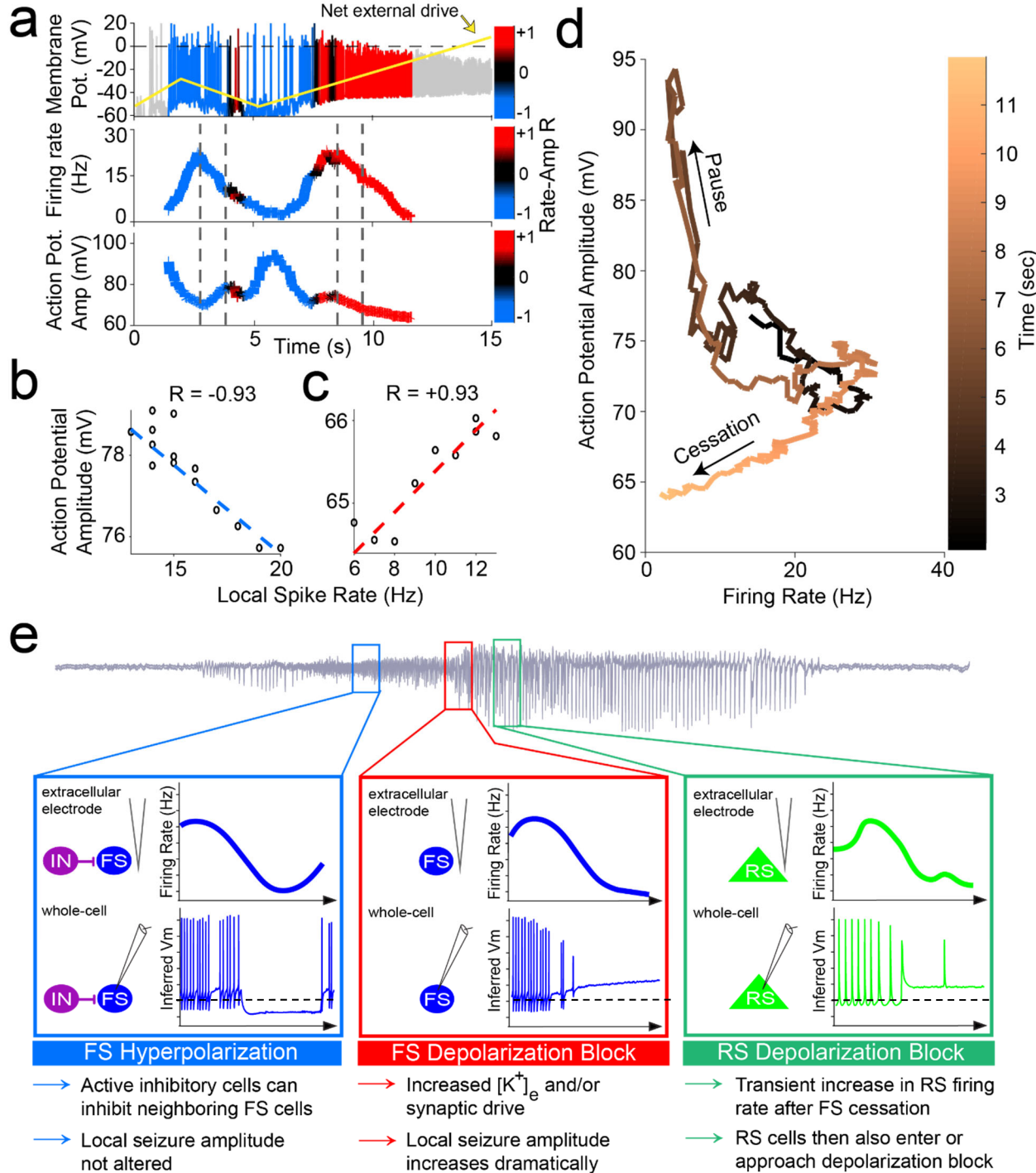
735  
736 **Figure 4. Cessation of individual FS unit activity is consistently associated with inferred**  
737 **membrane potential signatures of depolarization block, despite prior hyperpolarized pauses**

738  
739  
740  
741  
742  
743

- a. Firing rate (upper) and trough-to-peak spike amplitude (lower) of example FS unit in Patient A, color-coded by the local correlation between spike rate and amplitude (in 1 second time bins) as an extracellular proxy for membrane potential trajectory and subthreshold input history. Dotted lines indicate starts and ends of two time periods of firing rate suppression characterized by different membrane potential signatures further characterized in (B), namely a negative correlation regime corresponding to inhibition followed by a positive correlation regime

- 744 corresponding to over-excitation ending in firing rate cessation putatively though depolarization  
745 block.
- 746
- 747 b. Example of negative correlation (*left*) between local spike rate and amplitude in first time period  
748 indicated by dotted lines in (A) and example of positive correlation (*right*) between local spike rate  
749 and amplitude in second time period indicated by dotted lines in (A). Least squares linear fit  
750 indicated in dotted lines following color scheme in (A) with Pearson's correlation coefficient  
751 indicated above each plot.
- 752
- 753 c. Trajectory of unit activity over time during seizure in local spike rate vs spike amplitude space,  
754 with increasing time indicated by increasingly lighter copper color. The first time period of firing  
755 rate reduction in dotted lines in (A) is indicated with an arrow as "Pause" and the second time  
756 period of firing rate reduction in dotted lines in (A) is indicated with an arrow as "Cessation."
- 757
- 758 d. Firing rate of unit from (A) with neighboring FS unit firing rate overlaid, giving further evidence that  
759 first period of firing rate suppression corresponds to inhibition from local FS units while second  
760 period of firing rate suppression does not correspond to inhibition from local FS units.
- 761
- 762 e. Unit cessation-triggered population average of the time course of novel membrane potential  
763 regime measure, i.e. the correlation coefficient relating spiking amplitude and rate in a local time  
764 window, around the two significant descents in firing rate (below 30% of peak rate) that occur in  
765 sequence during seizure. These are designated as pause (*left panel*) and cessation (*right panel*).  
766 Left panel shows population average firing rate (blue) and inferred membrane potential regime  
767 (black) aligned according to the time of pause in each unit, for all FS units displaying a pause  
768 (n=14), with inset showing average for best-isolated FS units displaying a pause (n=10). Right  
769 panel shows population average firing rate (red) and inferred membrane potential regime (black)  
770 aligned according to the cessation time of each unit, for all FS units (n=37), with inset showing  
771 average for best-isolated FS units (n=24).
- 772
- 773 f. Probability distribution of membrane potential regime measure (spike rate-amplitude correlation;  
774 black line) at the time of pause (*left panel*) for FS unit pausing subpopulation (n=14) with sample  
775 mean distribution (gold line; resampling size n=10,  $N_{bootstrap}=50,000$ ) showing the mean  
776 correlation to be significantly below zero, i.e. in the hyperpolarized membrane potential regime  
777 (blue). In combination with its declining firing rate, this is indicative of widespread inhibition across  
778 this subpopulation at the time of pause. The population distribution of inferred membrane  
779 potential regime is also shown at the time of cessation (*right panel*) for the full FS unit population  
780 (n=37) with sample mean distribution (gold line; resampling size n=10,  $N_{bootstrap}=50,000$ ) showing  
781 the mean correlation to be significantly above zero, i.e. in the highly depolarized membrane  
782 potential regime (red). This is indicative of widespread depolarization block occurring across FS  
783 population at the time of cessation.
- 784
- 785 g. Unit cessation-triggered population average of the time course of same-electrode LFP amplitude  
786 around unit activity pause (*left panel*) and cessation (*right panel*). In particular, left panel shows  
787 population average firing rate (blue) and LFP amplitude (black) aligned according to the time of  
788 pause in each unit, for all FS units displaying a pause (n=14). Right panel shows population  
789 average firing rate (red) and LFP amplitude (black) aligned according to the time of cessation in  
790 each unit, for all FS units (n=37), indicative of larger LFP increase associated with second FS  
791 firing rate descent (cessation) than with first (pause) despite comparable local firing rates in the  
792 two conditions.

793



794

795  
796  
797  
798  
799  
800  
801  
802  
**Figure 5. Mechanistic model of unit dynamics across seizure progression: inhibition followed by**  
**over-excitation in conductance-based neuron model reproduces key features of extracellular unit**  
**behavior during seizures.**

- a. Simulated membrane potential in conductance-based spiking model color-coded by the local correlation between spike rate and amplitude and with net excitatory input indicated by dotted line. Shows what is hypothesized to be happening within cortical cells during seizure progression as inferred from extracellular spike shape and rate dynamics.

- 803       **b.** Firing rate (*upper*) and trough-to-peak spike amplitude (*lower*) of example FS unit in Patient A,  
804       color-coded by the local correlation between spike rate and amplitude as an extracellular proxy  
805       for membrane potential and subthreshold input history. Dotted lines indicate starts and ends of  
806       two time periods of firing rate suppression characterized by different membrane potential  
807       signatures further characterized in (B), namely a negative correlation regime corresponding to  
808       inhibition followed by a positive correlation regime corresponding to over-excitation ending in  
809       firing rate cessation putatively through depolarization block.  
810  
811       **c.** Example of negative correlation (*left*) between local spike rate and amplitude during firing pause  
812       in (A) and example of positive correlation (*right*) between local spike rate and amplitude during  
813       firing cessation. Least squares linear fit indicated in dotted lines following color scheme in (A) with  
814       Pearson's correlation coefficient indicated above each plot.  
815  
816       **d.** Trajectory of unit activity over time during seizure in local spike rate vs spike amplitude space,  
817       with increasing time indicated by increasingly lighter copper color. The first time period of firing  
818       rate reduction in (A) is indicated with an arrow as "Pause" and the second time period of firing  
819       rate reduction is indicated with an arrow as "Cessation."  
820  
821       **e. Summary of observed dynamics in cell-type specific firing rate and inferred membrane**  
822       **potential trajectories.**  
823       **Blue box:** Following seizure onset, some FS cells can stop firing for brief periods (as observed  
824       on extracellular electrodes, upper panel). This pause in firing is coupled with signs of  
825       hyperpolarization in the inferred membrane potential (lower panel).  
826       **Red box:** As the seizure starts to transition to a dramatically higher amplitude FS cells stop firing  
827       (as observed on extracellular electrodes, upper panel). This cessation is coupled with signs of  
828       excessive depolarization in the inferred membrane potential (lower panel; resting membrane  
829       potential indicated as dashed line). This is likely due to elevated extracellular potassium ion  
830       concentrations by this point of the seizure or increased synaptic drive.  
831       **Green box:** The subsequent stage of high amplitude spike-and-wave rhythms corresponds to a  
832       transient increase and then decrease of firing rate amongst RS cells (as observed on extracellular  
833       electrodes, upper panel). This decrease in firing rate is coupled with signs of excessive  
834       depolarization in the inferred membrane potential (lower panel).

835

836

837

838

839

840

841

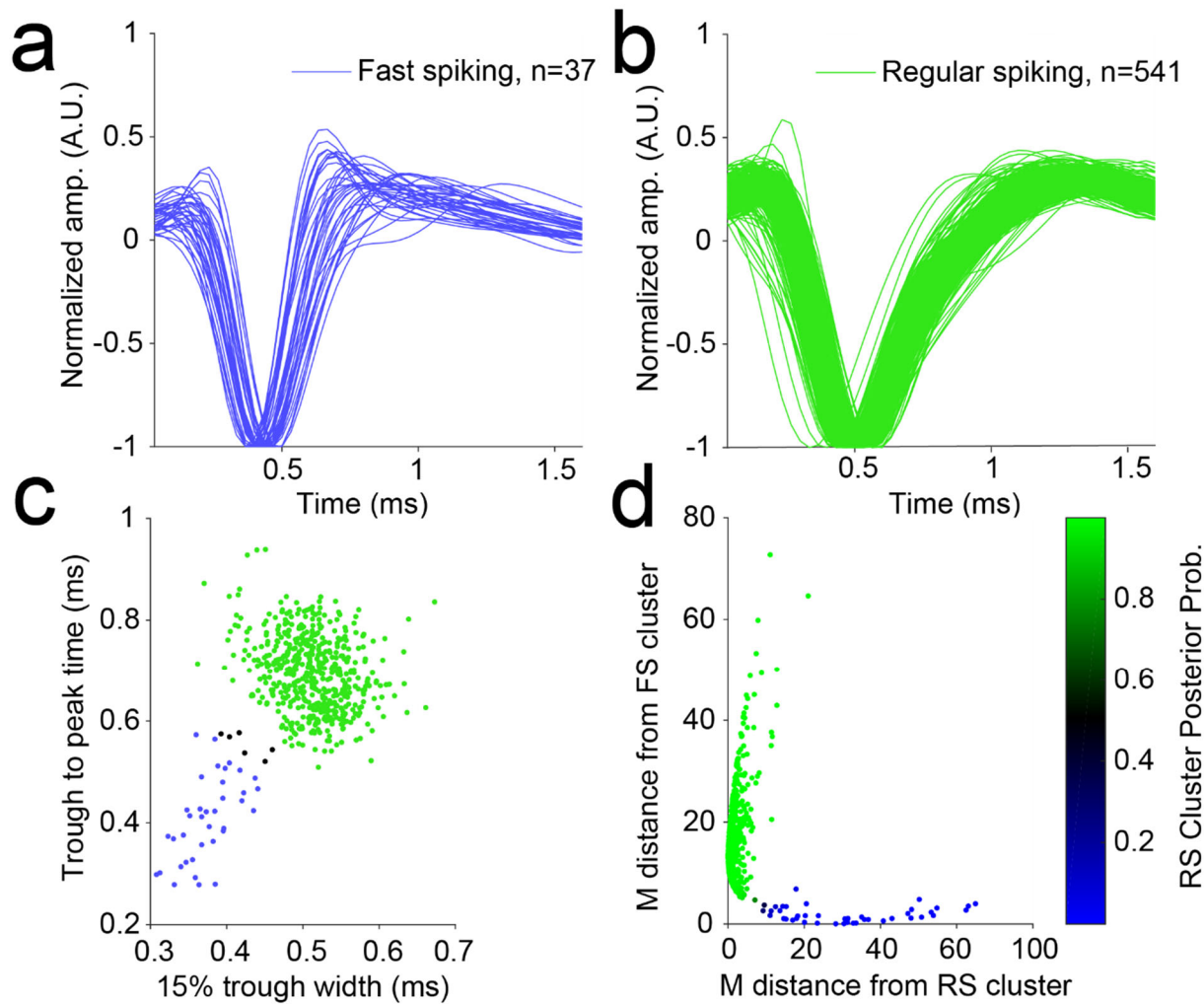
842

843

844

845

## SUPPLEMENTARY INFORMATION

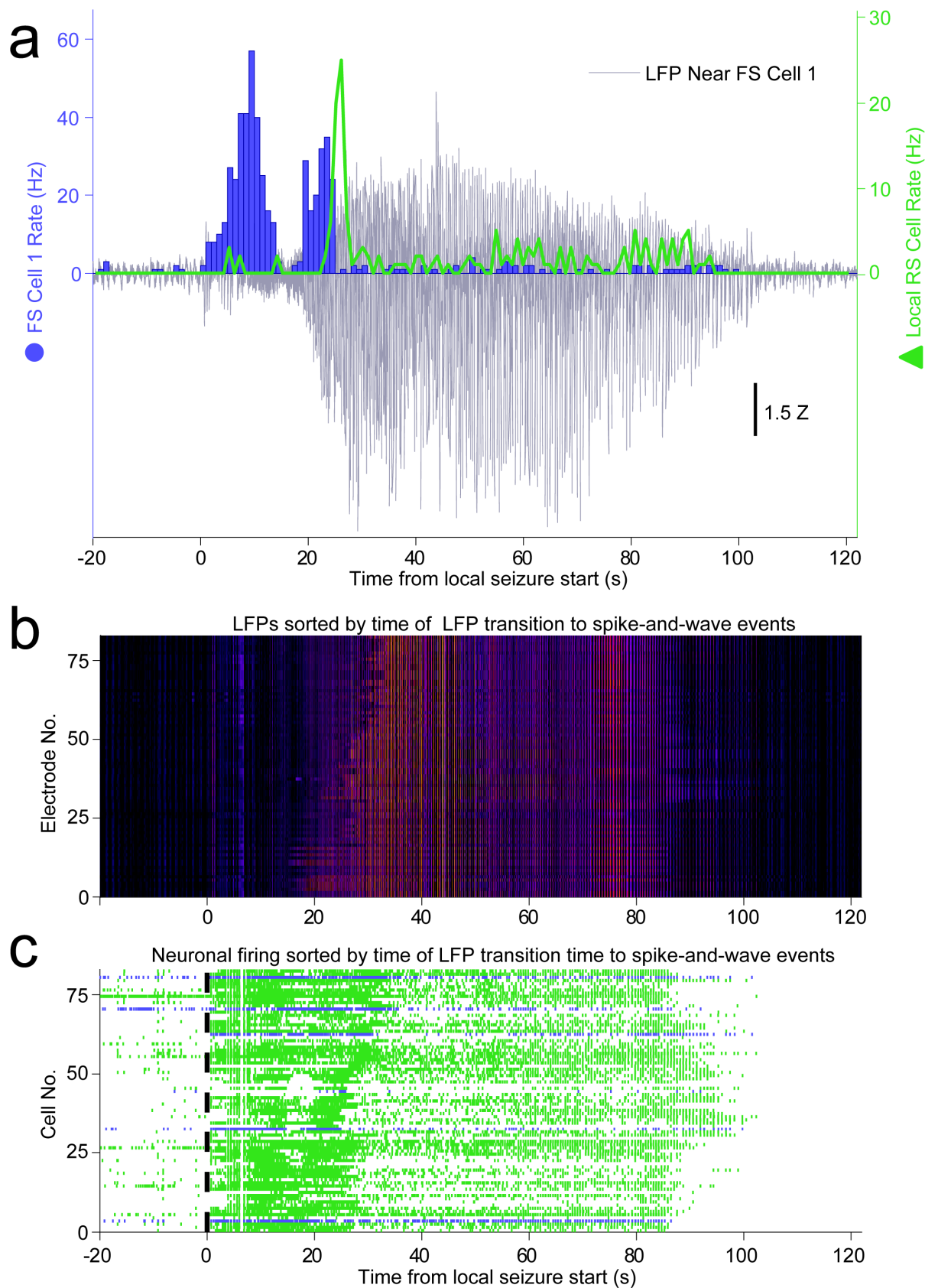


846

### Extended Data Figure 1: Human neural activity classification

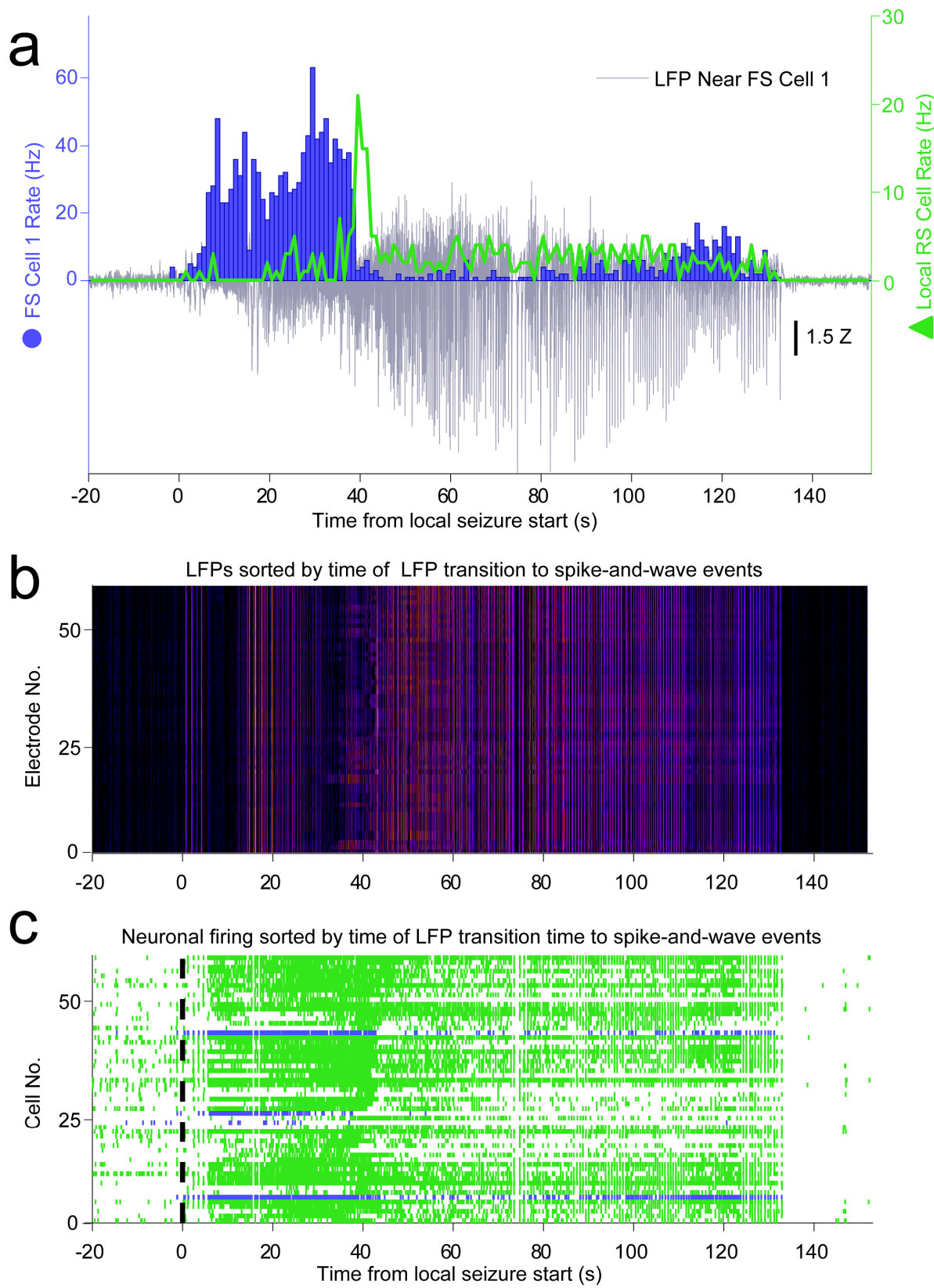
- Average waveform of each FS-classified unit, normalized by the value the waveform reaches at its trough. The overlaid average waveforms show visual consistency amongst all units classified as FS and as having spike widths narrower than those of RS-classified units.
- Average waveform of each RS-classified unit, normalized by the value the waveform reaches at its trough. The overlaid average waveforms show visual consistency amongst all units classified as RS and as having spike widths wider than those of FS-classified units.
- All units indicated as points in the average waveform feature space that produced optimal cluster separation, namely the width of the waveform at the potential corresponding to 15% of the potential at its trough and the time between the trough and peak of the waveform. Clustering was automated using a Gaussian Mixture Model where points with posterior probability exceeding 0.95 were assigned to the closest centroid. Black dots indicate units that did not exceed this threshold for either Gaussian cloud and were thus unclassified and not used in the remainder of the study.
- Mahalanobis distance of each unit from both the RS and FS clusters with color indicating its posterior probability of belonging to the RS cluster. Closeness of points to both axes shows that the clusters are well-separated when accounting for their different variances along different directions in feature space.

865



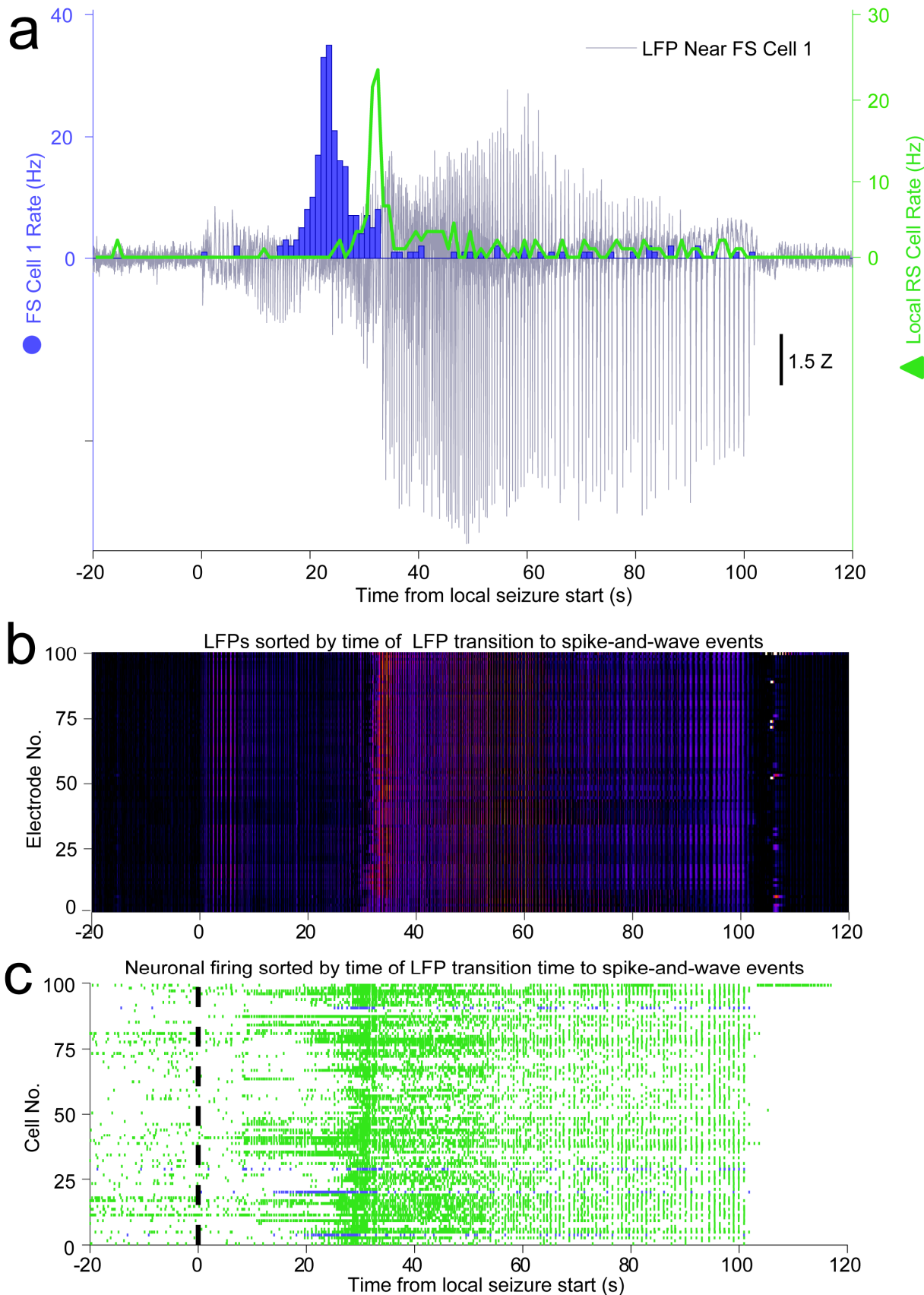
867   **Extended Data Figure 2: Human neocortical inhibitory and excitatory neuron activities have**  
868   **distinct temporal profiles relative to secondarily generalized focal seizure progression on local**  
869   **electrodes, Patient A, Seizure 2**

- 870   a. The LFP (gray) recorded at the same location as FS Cell 1 (blue) dramatically increases at the  
871   same time as FS Cell 1 decreases firing. FS Cell 1 activity cessation again precedes a sharp  
872   increase in local RS cell activity (green), further suggesting an important role of FS cells in  
873   controlling local activity during seizure progression.  
874   b. Heatmap shows local LFP amplitude (absolute value) over time on each electrode in NeuroPort  
875   array exhibiting classifiable units as each row, sorted by time of start of spike-and-wave event  
876   and with brighter colors indicating larger amplitudes.  
877   c. Raster plot showing spike times of all cells on NeuroPort array in Patient B that could be  
878   classified into FS (blue) or RS (green) categories with rows sorted by the same order as in (B).  
879   Note the increasing delay to reduction in spike density corresponding to LFP transition to spike-  
880   and-wave events suggesting control of local seizure progression by local cellular spiking activity.



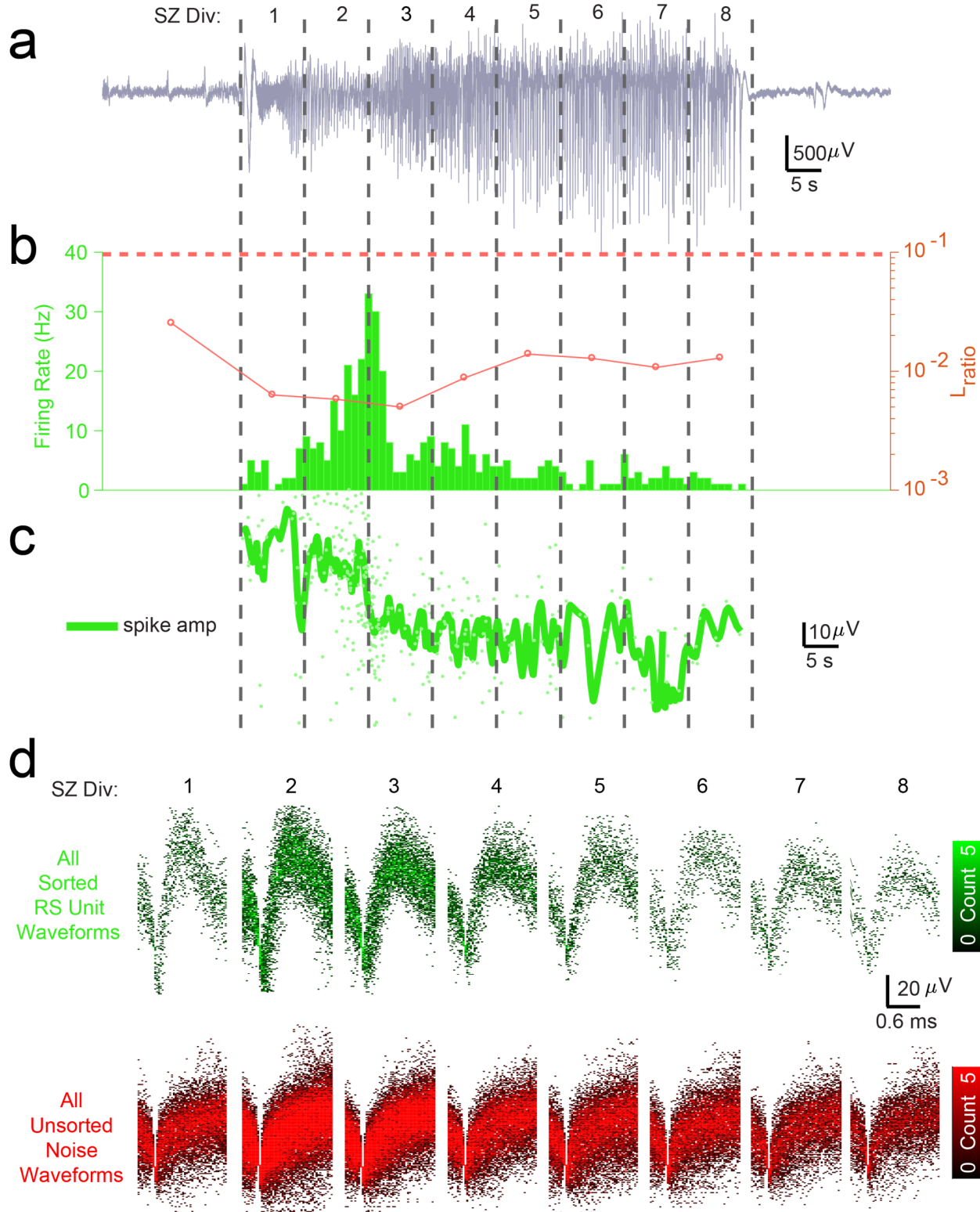
882   **Extended Data Figure 3: Human neocortical inhibitory and excitatory neuron activities have**  
883   **distinct temporal profiles relative to secondarily generalized focal seizure progression on local**  
884   **electrodes, Patient C, Seizure 2**

- 885   a. The LFP (gray) recorded at the same location as FS Cell 1 (blue) dramatically increases at the  
886   same time as FS Cell 1 decreases firing. FS Cell 1 activity cessation again precedes a sharp  
887   increase in local RS cell activity (green), further suggesting an important role of FS cells in  
888   controlling local activity during seizure progression.  
889   b. Heatmap shows local LFP amplitude (absolute value) over time on each electrode in NeuroPort  
890   array exhibiting classifiable units as each row, sorted by time of start of spike-and-wave event  
891   and with brighter colors indicating larger amplitudes.  
892   c. Raster plot showing spike times of all cells on NeuroPort array in Patient C that could be  
893   classified into FS (blue) or RS (green) categories with rows sorted by the same order as in (B).  
894   Note the increasing delay to reduction in spike density corresponding to LFP transition to spike-  
895   and-wave events suggesting control of local seizure progression by local cellular spiking activity.  
896



898   **Extended Data Figure 4: Human neocortical inhibitory and excitatory neuron activities have**  
899   **distinct temporal profiles relative to secondarily generalized focal seizure progression on local**  
900   **electrodes, Patient B, Seizure 1**

- 901   a. The LFP (gray) recorded at the same location as FS Cell 1 (blue) dramatically increases at the  
902   same time as FS Cell 1 decreases firing. FS Cell 1 activity cessation again precedes a sharp  
903   increase in local RS cell activity (green), further suggesting an important role of FS cells in  
904   controlling local activity during seizure progression.  
905   b. Heatmap shows local LFP amplitude (absolute value) over time on each electrode in NeuroPort  
906   array exhibiting classifiable units as each row, sorted by time of start of spike-and-wave event  
907   and with brighter colors indicating larger amplitudes.  
908   c. Raster plot showing spike times of all cells on NeuroPort array in Patient C that could be  
909   classified into FS (blue) or RS (green) categories with rows sorted by the same order as in (B).  
910

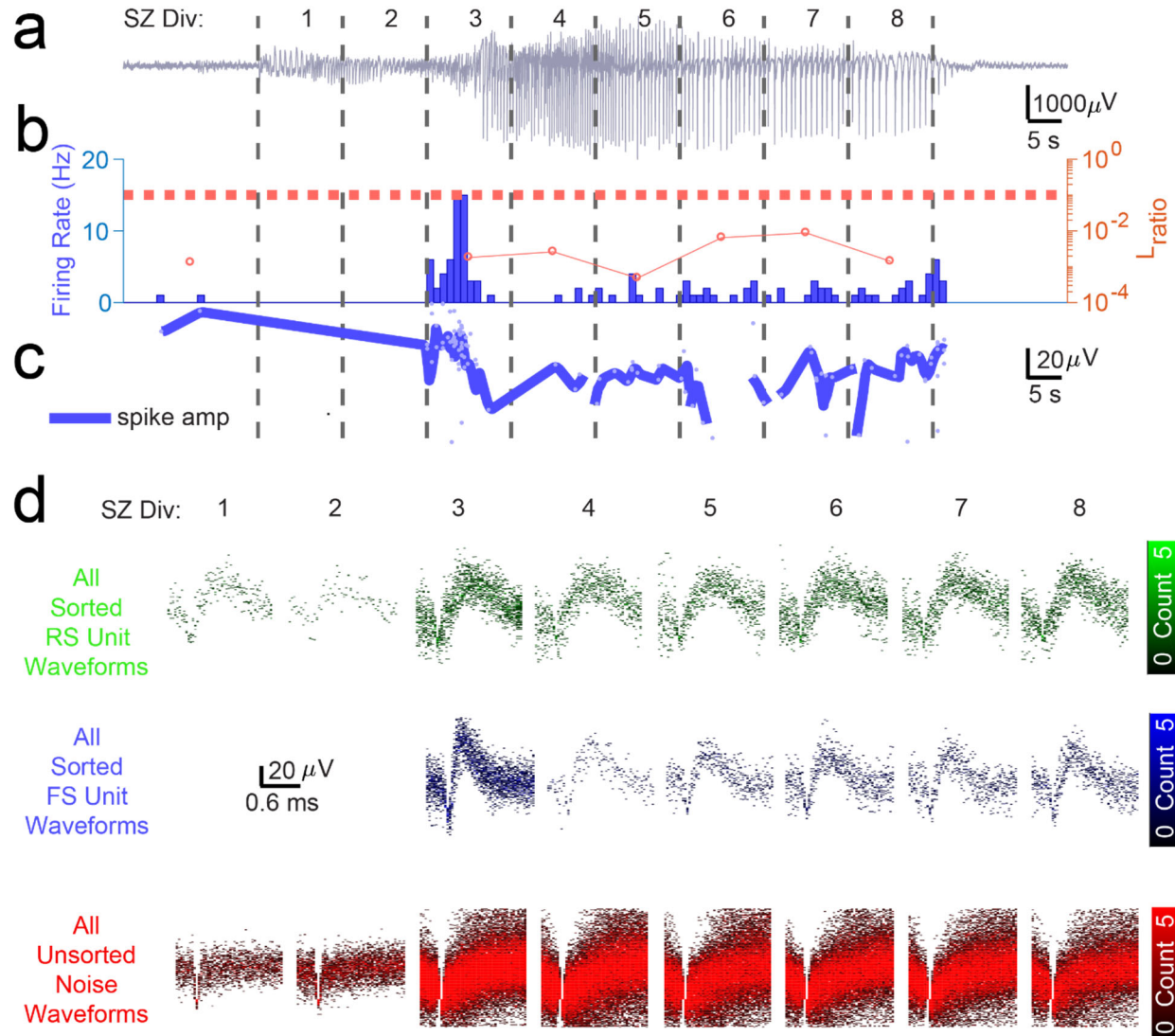


911

912 **Extended Data Figure 5: Cluster isolation quality assessment suggests RS units are well-**  
913 **isolatable across seizure despite changing unit amplitude and noise structure, allowing analysis**  
914 **of firing rate changes across seizure.**

- 915        a. LFP in Patient C indicating seizure as split into 8 equal time divisions for analysis of unit isolation  
916              quality across duration of seizure.  
917        b. Bar graph shows firing rate in 1 second bins of best-isolated example RS unit (green) in Patient  
918              C. Dotted red line indicates threshold used to determine best-isolated units using the dynamic  
919               $L_{ratio}$  measure (see Methods) in each time division of seizure. Line plot indicates dynamic  $L_{ratio}$  in  
920              each division and shows large separation of example FS unit from noise in feature space used for  
921              clustering throughout the seizure (note log scale).  
922        c. Line plot showing average spike amplitude (dark green) and individual spike amplitudes (light  
923              green) of example RS unit over course of seizure in Patient C. Note that even as amplitude  
924              decreases the unit remains well-isolated from noise as quantified by dynamic  $L_{ratio}$  across seizure.  
925        d. Time-voltage histogram of all threshold crossings assigned to this example RS unit (green,  
926              *Upper*) and to noise (red, *Lower*) in eight divisions of seizure in Patient C. Shows unit waveforms  
927              are visually distinguishable from threshold crossings assigned as noise across seizure.

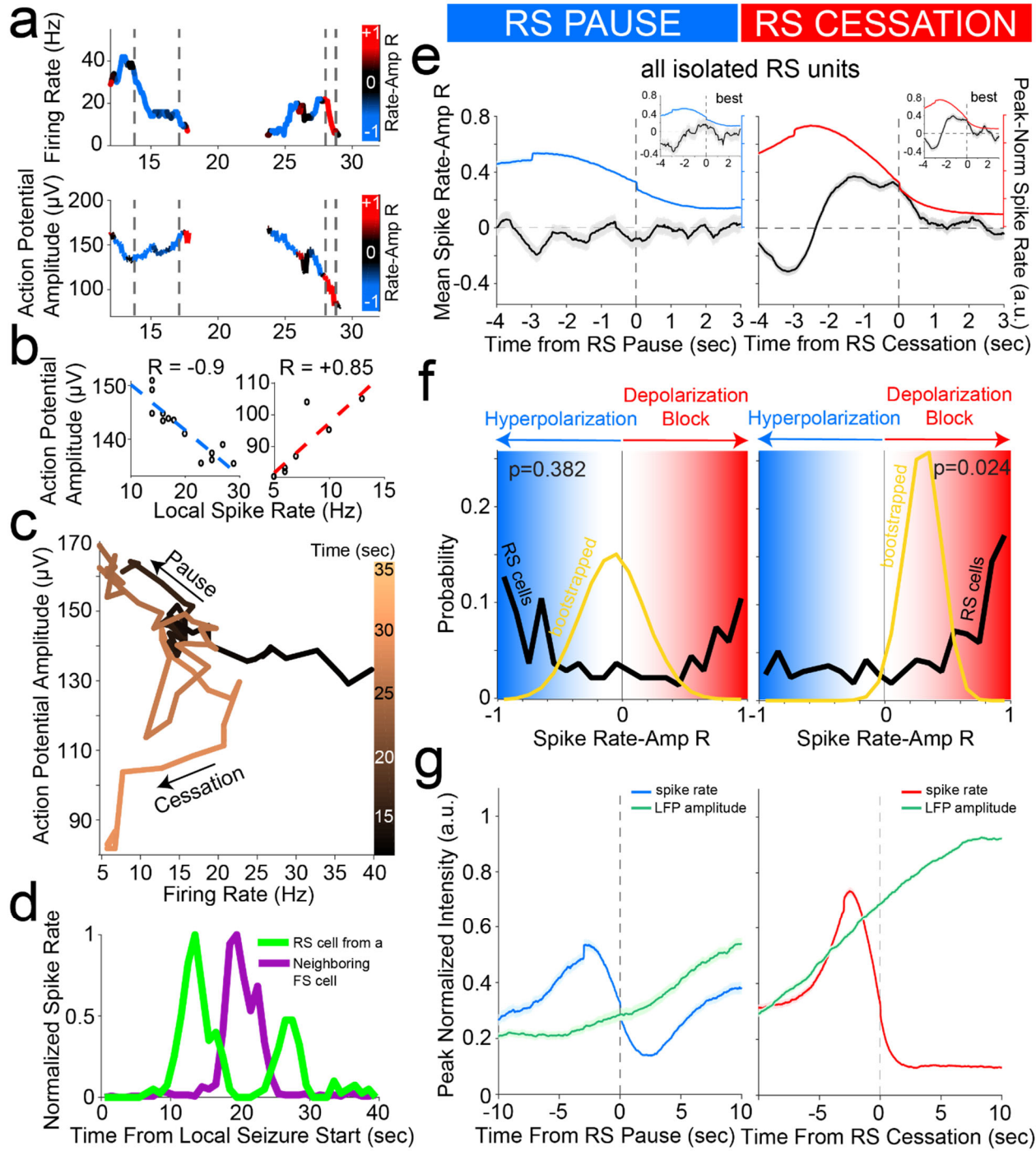
928  
929  
930  
931  
932  
933  
934



936   **Extended Data Figure 6: Cluster isolation quality assessment suggests RS and FS units on same**  
937   **channel are well-isolatable across seizure despite changing unit amplitude and noise structure,**  
938   **allowing analysis of firing rate changes across seizure for multiple patients.**

- 939   a. LFP in Patient B indicating seizure as split into 8 equal time divisions for analysis of unit isolation  
940   quality across duration of seizure.  
941   b. Bar graph shows firing rate in 1 second bins of best-isolated example FS unit (blue) in Patient B.  
942   Dotted red line indicates threshold used to determine best-isolated units using the dynamic  $L_{ratio}$   
943   measure (see Methods) in each time division of seizure. Line plot indicates dynamic  $L_{ratio}$  in each  
944   division and shows large separation of example FS unit from noise in feature space used for  
945   clustering throughout the seizure (note log scale).  
946   c. Line plot showing average spike amplitude (dark blue) and individual spike amplitudes (light blue)  
947   of example FS unit over course of seizure in Patient B. Note that even as amplitude decreases  
948   the unit remains well-isolated from noise as quantified by dynamic  $L_{ratio}$  across seizure.  
949   d. Time-voltage histogram of all threshold crossings assigned to example FS unit (blue, *Middle*), RS  
950   unit on same channel (green, *Upper*), and to noise (red, *Lower*) in eight divisions of seizure in  
951   Patient B. Shows unit waveforms are visually distinguishable from threshold crossings assigned  
952   as noise and as other units across seizure.

953



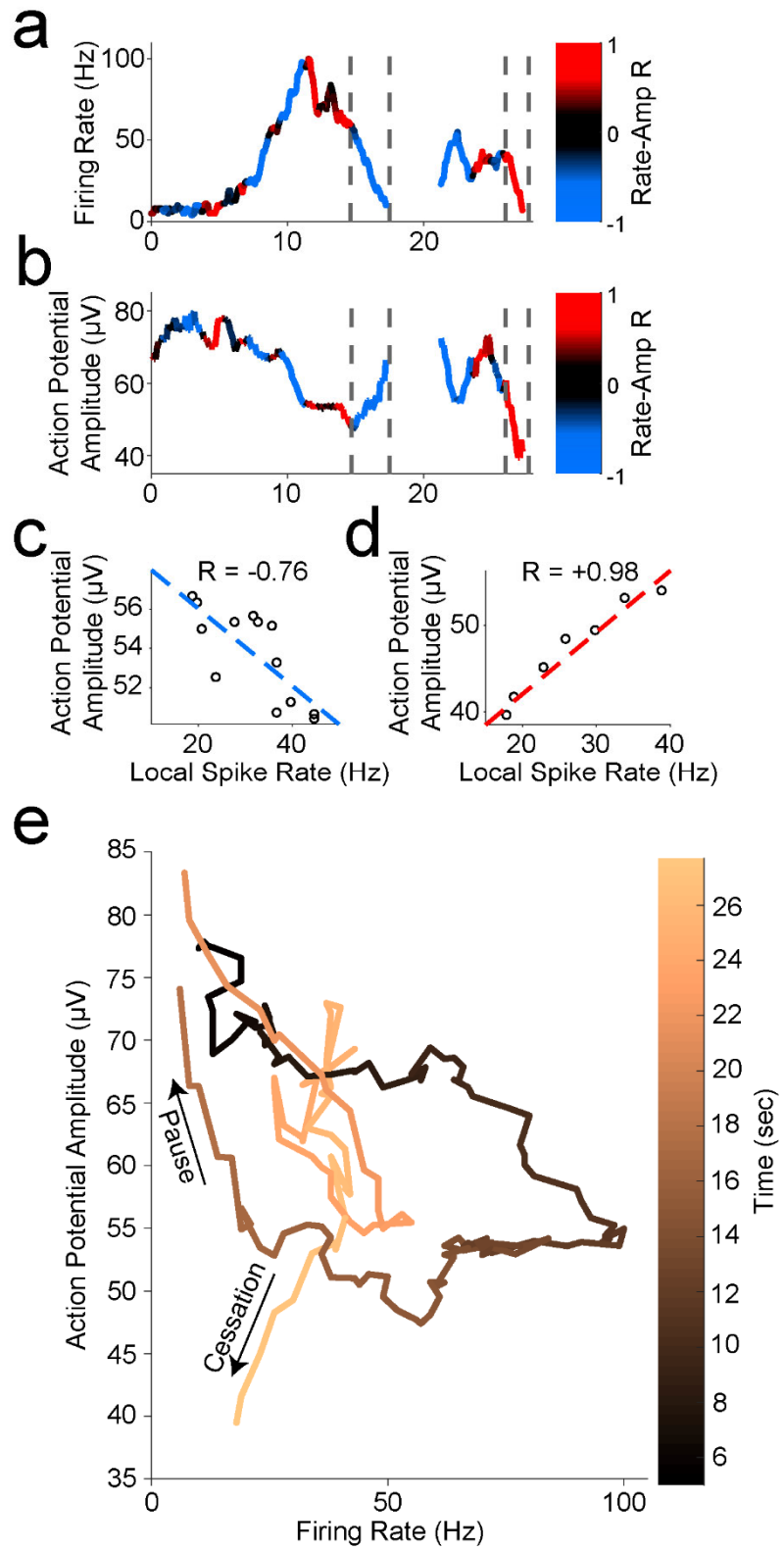
954

955 **Extended Data Figure 7: Cessation of individual RS unit activity is consistently associated with**  
 956 **inferred membrane potential signatures of depolarization block, despite prior pauses**

- 957 a. Firing rate (*upper*) and trough-to-peak spike amplitude (*lower*) of example RS unit in Patient A,  
 958 color-coded by the local correlation between spike rate and amplitude (in 1 second time bins) as  
 959 an extracellular proxy for membrane potential trajectory and subthreshold input history. Dotted  
 960 lines indicate starts and ends of two time periods of firing rate suppression characterized by  
 961 different membrane potential signatures further characterized in (B), namely a negative  
 962 correlation regime corresponding to inhibition followed by a positive correlation regime

- 963 corresponding to over-excitation ending in firing rate cessation putatively though depolarization  
964 block.
- 965 b. Example of negative correlation (*left*) between local spike rate and amplitude in first time period  
966 indicated by dotted lines in (A) and example of positive correlation (*right*) between local spike rate  
967 and amplitude in second time period indicated by dotted lines in (A). Least squares linear fit  
968 indicated in dotted lines following color scheme in (A) with Pearson's correlation coefficient  
969 indicated above each plot.
- 970 c. Trajectory of unit activity over time during seizure in local spike rate vs spike amplitude space,  
971 with increasing time indicated by increasingly lighter copper color. The first time period of firing  
972 rate reduction in dotted lines in (A) is indicated with an arrow as "Pause" and the second time  
973 period of firing rate reduction in dotted lines in (A) is indicated with an arrow as "Cessation."
- 974 d. Firing rate of unit from (A) with neighboring FS unit firing rate overlaid, giving further evidence that  
975 first period of firing rate suppression corresponds to inhibition from local FS units while second  
976 period of firing rate suppression does not correspond to inhibition from local FS units.
- 977 e. Unit cessation-triggered population average of the time course of novel membrane potential  
978 regime measure, i.e. the correlation coefficient relating spiking amplitude and rate in a local time  
979 window, around the two significant descents in firing rate (below 30% of peak rate) that occur in  
980 sequence during seizure. These are designated as pause (*left panel*) and cessation (*right panel*).  
981 Left panel shows population average firing rate (blue) and inferred membrane potential regime  
982 (black) aligned according to the time of pause in each unit, for all RS units displaying a pause  
983 (n=176), with inset showing average for best-isolated RS units displaying a pause (n=41). Right  
984 panel shows population average firing rate (red) and inferred membrane potential regime (black)  
985 aligned according to the cessation time of each unit, for all RS units meeting cessation criteria  
986 (n=379), with inset showing average for best-isolated RS units (n=111).
- 987 f. Probability distribution of membrane potential regime measure (spike rate-amplitude correlation;  
988 black line) at the time of pause (*left panel*) for RS unit pausing subpopulation (n=176) with sample  
989 mean distribution (gold line; resampling size n=10,  $N_{bootstrap}=50,000$ ) showing a bimodal  
990 distribution of correlation coefficients near +1 and -1, i.e. in the hyperpolarized membrane  
991 potential regime (blue) or in the highly depolarized regime (red). The population distribution of  
992 inferred membrane potential regime is also shown at the time of cessation (*right panel*) for the RS  
993 unit population meeting cessation criteria (n=379) with sample mean distribution (gold line;  
994 resampling size n=10,  $N_{bootstrap}=50,000$ ) showing the mean correlation to be significantly above  
995 zero, i.e. in the highly depolarized membrane potential regime (red). This is indicative of  
996 widespread depolarization block occurring across RS population at the time of cessation.
- 997 g. Unit cessation-triggered population average of the time course of same-electrode LFP amplitude  
998 around unit activity pause (*left panel*) and cessation (*right panel*). In particular, left panel shows  
999 population average firing rate (blue) and LFP amplitude (black) aligned according to the time of  
1000 pause in each unit, for all RS units displaying a pause (n=176). Right panel shows population  
1001 average firing rate (red) and LFP amplitude (black) aligned according to the time of cessation in  
1002 each unit, for all RS units (n=379).

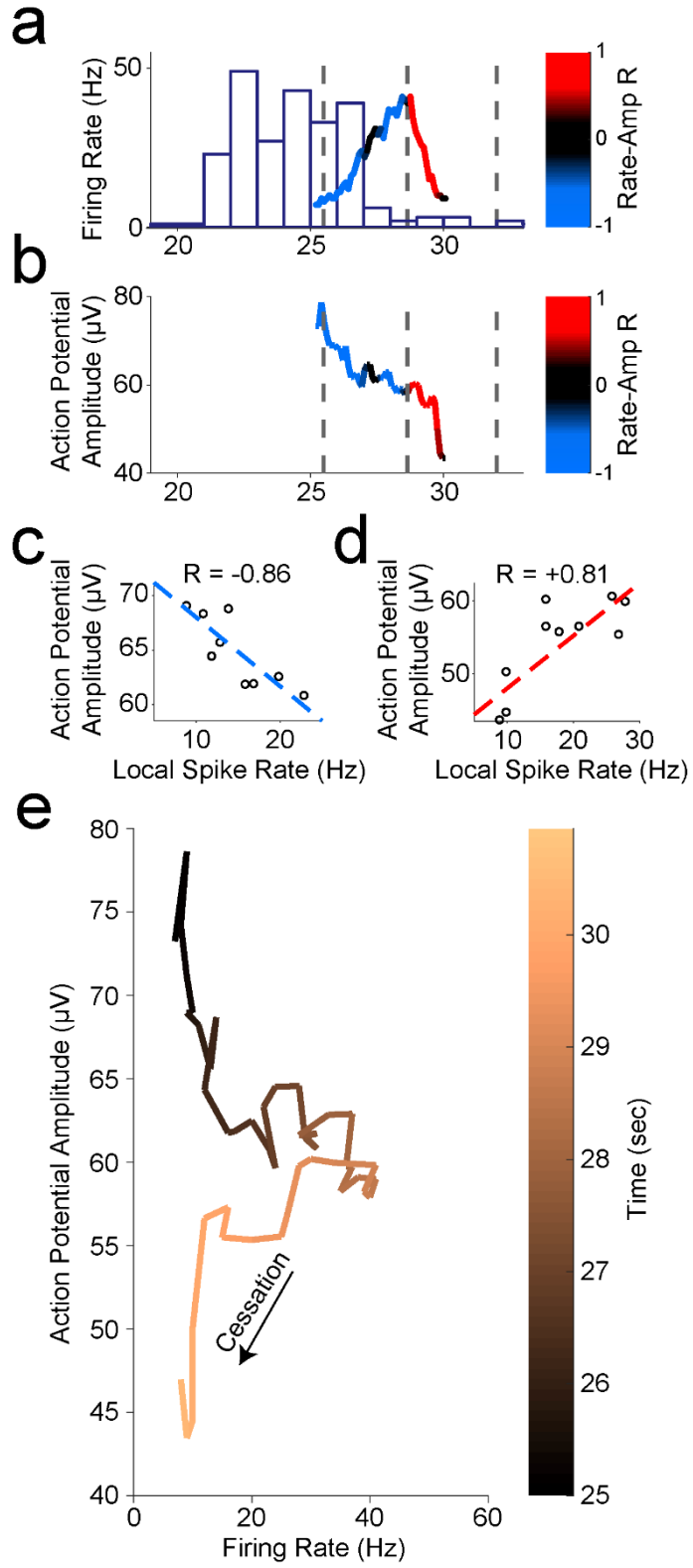
1003



1005   **Extended Data Figure 8: Seizure progression is consistently associated with extracellular signs of**  
1006   **depolarization block preceded by inhibition in single units.**

- 1007   a. Firing rate (*upper*) and trough-to-peak spike amplitude (*lower*) of another example FS unit in  
1008   Patient A, color-coded by the local correlation between spike rate and amplitude (in 1 second  
1009   time bins) as an extracellular proxy for membrane potential and subthreshold input history.  
1010   Dotted lines indicate starts and ends of two time periods of firing rate suppression characterized  
1011   by different membrane potential signatures further characterized in (B), namely a negative  
1012   correlation regime corresponding to inhibition followed by a positive correlation regime  
1013   corresponding to over-excitation ending in firing rate cessation putatively through depolarization  
1014   block.  
1015   b. Example of negative correlation (*left*) between local spike rate and amplitude in first time period  
1016   indicated by dotted lines in (A) and example of positive correlation (*right*) between local spike rate  
1017   and amplitude in second time period indicated by dotted lines in (A). Least squares linear fit  
1018   indicated in dotted lines following color scheme in (A) with Pearson's correlation coefficient  
1019   indicated above each plot.  
1020   c. Trajectory of unit activity over time during seizure in local spike rate vs spike amplitude space,  
1021   with increasing time indicated by increasingly lighter copper color. The first time period of firing  
1022   rate reduction in dotted lines in (A) is indicated with an arrow as "Pause" and the second time  
1023   period of firing rate reduction in dotted lines in (A) is indicated with an arrow as "Cessation."

1024



1026   **Extended Data Figure 9: Seizure progression is consistently associated with extracellular signs of**  
1027   **depolarization block preceded by inhibition in single units.**

- 1028   a. Firing rate (*upper*) and trough-to-peak spike amplitude (*lower*) of another example RS unit in  
1029   Patient A, color-coded by the local correlation between spike rate and amplitude (in 1 second  
1030   time bins) as an extracellular proxy for membrane potential and subthreshold input history. Firing  
1031   rate of local FS unit is overlaid as purple histogram. Dotted lines indicate start and end times of  
1032   two time periods of firing rate suppression characterized by different membrane potential  
1033   signatures further characterized in (B), namely a negative correlation regime corresponding to  
1034   inhibition followed by a positive correlation regime corresponding to over-excitation ending in  
1035   firing rate cessation putatively through depolarization block.  
1036   b. Example of negative correlation (*left*) between local spike rate and amplitude in first time period  
1037   indicated by dotted lines in (A) and example of positive correlation (*right*) between local spike rate  
1038   and amplitude in second time period indicated by dotted lines in (A). Least squares linear fit  
1039   indicated in dotted lines following color scheme in (A) with Pearson's correlation coefficient  
1040   indicated above each plot.  
1041   c. Trajectory of unit activity over time during seizure in local spike rate vs spike amplitude space,  
1042   with increasing time indicated by increasingly lighter copper color. RS unit is released from  
1043   inhibition shortly following the cessation of activity in local FS unit as indicated by increasing firing  
1044   rate with decreasing amplitude but then enters regime of over-excitation indicated by decreasing  
1045   firing rate with decreasing amplitude at trajectory "corner" corresponding to a spiking rate of 40  
1046   Hz, until the unit ceases to fire likely due to depolarization block given these indicators of  
1047   membrane potential history.

1048  
1049

1050

1051

1052

1053

1054

1055

1056

1057

1058

1059

1060

1061

1062

1063 **REFERENCES**

1064

- 1065 1. Annegers, J. F. The Treatment of Epilepsy: Principles and Practice. (Third  
1066 Edition). in *The Treatment of Epilepsy: Principles and Practice* (ed. Wyllie, E.) 131–  
1067 138 (Wiley, 2001). doi:10.1002/hup.372
- 1068 2. Thurman, D. J. et al. Standards for epidemiologic studies and surveillance of  
1069 epilepsy. *Epilepsia* **52**, 2–26 (2011).
- 1070 3. Žiburkus, J., Cressman, J. R. & Schiff, S. J. Seizures as imbalanced up states:  
1071 excitatory and inhibitory conductances during seizure-like events. *J. Neurophysiol.*  
1072 **109**, 1296–1306 (2013).
- 1073 4. Farrell, J. S., Nguyen, Q.-A. & Soltesz, I. Review Resolving the Micro-Macro  
1074 Disconnect to Address Core Features of Seizure Networks. *Neuron* **101**, 1016–  
1075 1028 (2019).
- 1076 5. Elahian, B. et al. Low-voltage fast seizures in humans begin with increased  
1077 interneuron firing. *Ann. Neurol.* **84**, 588–600 (2018).
- 1078 6. Weiss, S. A. et al. Ictal onset patterns of local field potentials, high frequency  
1079 oscillations, and unit activity in human mesial temporal lobe epilepsy. *Epilepsia*  
1080 **57**, 111–121 (2016).
- 1081 7. Schwartzkroin, P. A. & Prince, D. A. Changes in excitatory and inhibitory synaptic  
1082 potentials leading to epileptogenic activity. *Brain Res.* **183**, 61–77 (1980).
- 1083 8. Gutnick, M. J., Connors, B. W. & Prince, D. A. Mechanisms of neocortical  
1084 epileptogenesis in vitro. *J. Neurophysiol.* **48**, 1321–1335 (1982).
- 1085 9. Prince, D. A. & Connors, B. W. Mechanisms of epileptogenesis in cortical  
1086 structures. *Ann. Neurol.* **16**, S59–S64 (1984).
- 1087 10. McCormick, D. A., Connors, B. W., Lighthall, J. W. & Prince, D. A. Comparative  
1088 electrophysiology of pyramidal and sparsely spiny stellate neurons of the  
1089 neocortex. *J. Neurophysiol.* **54**, 782–806 (1985).
- 1090 11. Chagnac-Amitai, Y. & Connors, B. W. Horizontal spread of synchronized activity  
1091 in neocortex and its control by GABA-mediated inhibition. *J. Neurophysiol.* **61**,  
1092 747–758 (1989).
- 1093 12. Ziburkus, J., Cressman, J. R., Barreto, E. & Schiff, S. J. Interneuron and  
1094 pyramidal cell interplay during in vitro seizure-like events. *J. Neurophysiol.* **95**,  
1095 3948–3954 (2006).
- 1096 13. Trevelyan, A. J. & Schevon, C. A. How inhibition influences seizure propagation.  
1097 *Neuropharmacology* **69**, 45–54 (2013).
- 1098 14. Karlócai, M. R. et al. Physiological sharp wave-ripples and interictal events in  
1099 vitro: what's the difference? *Brain* **137**, 463–85 (2014).
- 1100 15. Pavlov, I. & Walker, M. C. Tonic GABA<sub>A</sub> receptor-mediated signalling in temporal  
1101 lobe epilepsy. *Neuropharmacology* **69**, 55–61 (2013).
- 1102 16. Avoli, M. & de Curtis, M. GABAergic synchronization in the limbic system and its  
1103 role in the generation of epileptiform activity. *Progress in Neurobiology* **95**, 104–  
1104 132 (2011).
- 1105 17. Cope, D. W. et al. Enhanced tonic GABA<sub>A</sub> inhibition in typical absence epilepsy.  
1106 *Nat. Med.* **15**, 1392–1398 (2009).

- 1107 18. Neumann, A. R. *et al.* Involvement of fast-spiking cells in ictal sequences during  
1108 spontaneous seizures in rats with chronic temporal lobe epilepsy. *Brain* **140**,  
1109 2355–2369 (2017).
- 1110 19. Sessolo, M. *et al.* Parvalbumin-positive inhibitory interneurons oppose  
1111 propagation but favor generation of focal epileptiform activity. *J. Neurosci.* **35**,  
1112 9544–9557 (2015).
- 1113 20. Lévesque, M., Herrington, R., Hamidi, S. & Avoli, M. Interneurons spark seizure-  
1114 like activity in the entorhinal cortex. *Neurobiol. Dis.* **87**, 91–101 (2016).
- 1115 21. Khoshkho, S., Vogt, D. & Sohal, V. S. Dynamic, Cell-Type-Specific Roles for  
1116 GABAergic Interneurons in a Mouse Model of Optogenetically Inducible Seizures.  
1117 *Neuron* **93**, 291–298 (2017).
- 1118 22. Xu, H., Jeong, H. Y., Tremblay, R. & Rudy, B. Neocortical Somatostatin-  
1119 Expressing GABAergic Interneurons Disinhibit the Thalamorecipient Layer 4.  
1120 *Neuron* **77**, 155–167 (2013).
- 1121 23. Buckmaster, P. S., Jongen-Rêlo, A. L., Davari, S. B. & Wong, E. H. Testing the  
1122 disinhibition hypothesis of epileptogenesis in vivo and during spontaneous  
1123 seizures. *J. Neurosci.* **20**, 6232–40 (2000).
- 1124 24. Miri, M. L., Vinck, M., Pant, R. & Cardin, J. A. Altered hippocampal interneuron  
1125 activity precedes ictal onset. *Elife* **7**, (2018).
- 1126 25. Cammarota, M., Losi, G., Chiavegato, A., Zonta, M. & Carmignoto, G. Fast  
1127 spiking interneuron control of seizure propagation in a cortical slice model of focal  
1128 epilepsy. *J. Physiol.* **591**, 807–822 (2013).
- 1129 26. Petersen, C. C. H. Whole-Cell Recording of Neuronal Membrane Potential during  
1130 Behavior. *Neuron* **95**, 1266–1281 (2017).
- 1131 27. Nowak, L. G., Azouz, R., Sanchez-Vives, M. V., Gray, C. M. & McCormick, D. A.  
1132 Electrophysiological classes of cat primary visual cortical neurons in vivo as  
1133 revealed by quantitative analyses. *J. Neurophysiol.* **89**, 1541–1566 (2003).
- 1134 28. Cardin, J. A. *et al.* Driving fast-spiking cells induces gamma rhythm and controls  
1135 sensory responses. *Nature* **459**, 663–667 (2009).
- 1136 29. Rudy, B., Fishell, G., Lee, S. H. & Hjerling-Leffler, J. Three groups of interneurons  
1137 account for nearly 100% of neocortical GABAergic neurons. *Dev. Neurobiol.* **71**,  
1138 45–61 (2011).
- 1139 30. Connors, B. W., Pinto, D. J. & Telleian, A. E. Local pathways of seizure  
1140 propagation in neocortex. *Int. Rev. Neurobiol.* **45**, 527–46 (2001).
- 1141 31. Merricks, E. M. *et al.* Single unit action potentials in humans and the effect of  
1142 seizure activity. *Brain* **138**, 2891–906 (2015).
- 1143 32. Schevon, C. A. *et al.* Evidence of an inhibitory restraint of seizure activity in  
1144 humans. *Nat. Commun.* **3**, 1060 (2012).
- 1145 33. Sabolek, H. R. *et al.* A candidate mechanism underlying the variance of interictal  
1146 spike propagation. *J. Neurosci.* **32**, 3009–3021 (2012).
- 1147 34. Chervin, R. D., Pierce, P. A. & Connors, B. W. Periodicity and directionality in the  
1148 propagation of epileptiform discharges across neocortex. *J. Neurophysiol.* **60**,  
1149 1695–1713 (1988).
- 1150 35. Wong, B. Y. & Prince, D. A. The lateral spread of ictal discharges in neocortical  
1151 brain slices. *Epilepsy Res.* **7**, 29–39
- 1152 36. Golomb, D. & Amitai, Y. Propagating neuronal discharges in neocortical slices:

- 1153              Computational and experimental study. *J. Neurophysiol.* **78**, 1199–1211 (1997).
- 1154    37. Liou, J. Y. *et al.* A model for focal seizure onset, propagation, evolution, and  
1155              progression. *Elife* **9**, (2020).
- 1156    38. Martina, M., Schultz, J. H., Ehmke, H., Monyer, H. & Jonas, P. Functional and  
1157              molecular differences between voltage-gated K<sup>+</sup> channels of fast-spiking  
1158              interneurons and pyramidal neurons of rat hippocampus. *J. Neurosci.* **18**, 8111–  
1159              8125 (1998).
- 1160    39. Rudy, B. & McBain, C. J. Kv3 channels: Voltage-gated K<sup>+</sup> channels designed for  
1161              high-frequency repetitive firing. *Trends in Neurosciences* **24**, 517–526 (2001).
- 1162    40. Lien, C. C. & Jonas, P. Kv3 potassium conductance is necessary and kinetically  
1163              optimized for high-frequency action potential generation in hippocampal  
1164              interneurons. *J. Neurosci.* **23**, 2058–2068 (2003).
- 1165    41. Somjen, G. G. *Ions in the brain : normal function, seizures, and stroke*. (Oxford  
1166              University Press, 2004).
- 1167    42. Fröhlich, F., Bazhenov, M., Iragui-Madoz, V. & Sejnowski, T. J. Reviews:  
1168              Potassium dynamics in the epileptic cortex: New insights on an old topic.  
1169              *Neuroscientist* **14**, 422–433 (2008).
- 1170    43. Cruikshank, S. J., Lewis, T. J. & Connors, B. W. Synaptic basis for intense  
1171              thalamocortical activation of feedforward inhibitory cells in neocortex. *Nat.  
1172              Neurosci.* **10**, 462–468 (2007).
- 1173    44. Pouille, F. & Scanziani, M. Routing of spike series by dynamic circuits in the  
1174              hippocampus. *Nature* **429**, 717–723 (2004).
- 1175    45. Markram, H. *et al.* Interneurons of the neocortical inhibitory system. *Nature  
1176              Reviews Neuroscience* **5**, 793–807 (2004).
- 1177    46. Kawaguchi, Y. Physiological subgroups of nonpyramidal cells with specific  
1178              morphological characteristics in layer II/III of rat frontal cortex. *J. Neurosci.* **15**,  
1179              2638–2655 (1995).
- 1180    47. Kramer, M. A. *et al.* Human seizures self-terminate across spatial scales via a  
1181              critical transition. *Proc. Natl. Acad. Sci. U. S. A.* **109**, 21116–21121 (2012).
- 1182    48. Beverlin, B., Kakalios, J., Nykamp, D. & Netoff, T. I. Dynamical changes in  
1183              neurons during seizures determine tonic to clonic shift. *J. Comput. Neurosci.* **33**,  
1184              41–51 (2012).
- 1185    49. Fröhlich, F., Sejnowski, T. J. & Bazhenov, M. Network bistability mediates  
1186              spontaneous transitions between normal and pathological brain states. *J.  
1187              Neurosci.* **30**, 10734–10743 (2010).
- 1188    50. Blumenfeld, H. Cellular and network mechanisms of spike-wave seizures.  
1189              *Epilepsia* **46**, 21–33 (2005).
- 1190    51. Berényi, A., Belluscio, M., Mao, D. & Buzsáki, G. Closed-loop control of epilepsy  
1191              by transcranial electrical stimulation. *Science (80-. ).* **337**, 735–737 (2012).
- 1192    52. Wykes, R. C. *et al.* Epilepsy: Optogenetic and potassium channel gene therapy in  
1193              a rodent model of focal neocortical epilepsy. *Sci. Transl. Med.* **4**, (2012).
- 1194    53. Paz, J. T. *et al.* Closed-loop optogenetic control of thalamus as a tool for  
1195              interrupting seizures after cortical injury. *Nat. Neurosci.* **16**, 64–70 (2013).
- 1196    54. Krook-Magnuson, E., Armstrong, C., Oijala, M. & Soltesz, I. On-demand  
1197              optogenetic control of spontaneous seizures in temporal lobe epilepsy. *Nat.  
1198              Commun.* **4**, 1–8 (2013).

- 1199 55. Sukhotinsky, I. et al. Optogenetic Delay of Status Epilepticus Onset in an In Vivo  
1200 Rodent Epilepsy Model. *PLoS One* **8**, (2013).
- 1201 56. Bikson, M., Hahn, P. J., Fox, J. E. & Jefferys, J. G. R. Depolarization block of  
1202 neurons during maintenance of electrographic seizures. *J. Neurophysiol.* **90**,  
1203 2402–2408 (2003).
- 1204 57. Hoffman, D. A., Magee, J. C., Colbert, C. M. & Johnston, D. K+ channel regulation  
1205 of signal propagation in dendrites of hippocampal pyramidal neurons. *Nature* **387**,  
1206 869–875 (1997).
- 1207 58. Schmitzer-Torbert, N., Jackson, J., Henze, D., Harris, K., & Redish, A. D.  
1208 Quantitative measures of cluster quality for use in extracellular recordings.  
1209 *Neuroscience* **131**, 1-11 (2005).
- 1210 59. Magloire, V., Mercier, M. S., Kullmann, D. M., & Pavlov, I. GABAergic  
1211 interneurons in seizures: Investigating causality with optogenetics. *The  
1212 Neuroscientist* **25**, 344-358 (2019).
- 1213 60. De Polavieja, G. G., Harsch, A., Kleppe, I., Robinson, H. P. C. & Juusola, M.  
1214 Stimulus history reliably shapes action potential waveforms of cortical neurons. *J.  
1215 Neurosci.* **25**, 5657–5665 (2005).
- 1216  
1217  
1218  
1219  
1220  
1221  
1222  
1223